DISSECTING THE ENTORHINAL-HIPPOCAMPAL CIRCUITRY

MARIAMA BINETOU LAYE SECK

Thesis submitted to the University of Ottawa
in partial Fulfillment of the requirements for the
Master's degree in Neurosciences

Department Cellular and Molecular Medicine
Faculty of Medicine
University of Ottawa

© Mariama Binetou Laye Seck, Ottawa, Canada, 2026

Table of contents

List of Figures iv
List of Tables v
Abbreviations vi
Abstract vii
Acknowledgement viii
1. Introduction 1
1.1. Entorhinal cortex 1
1.2. Hippocampus 3
1.2.1. Dentate Gyrus 4
1.2.2. CA3 5
1.2.3. Pattern Separation 7
1.2.4. Pattern Completion 8
1.3. Neuronal tracing 10
2. Objective and Significance 12
2.1. Quantification methods between Entorhinal Cortex and Dentate Gyrus 12
2.2. Collateral connectivity of Layer II Entorhinal neurons 14
3. Methods 15
3.1. Animals 15
3.2. Stereotaxic Injection 15
3.3. Perfusion 16
3.4. Anterograde tracing 18
3.5. Retrograde tracing 20
3.5.1. Monosynaptic AAV mapping 20
3.5.2. Monosynaptic viral double-labeling 20
3.5.3. Monosynaptic non-viral double labelling 21
3.6. Slicing 22
3.6.1. Vibratome 22
3.6.2. Microtome 22
3.7. Immunofluorescence 22
3.8. Imaging 23
4.1. Retrograde AAV tracers allowing for sparse labeling of GCs in the DG 24

4.2. Injections in the entorhinal cortex 30
4.2.1 AAV anterogradely travel from the EC but fail to cross synapse in DG 30
4.2.2. Anterograde labeling of EC using HSV injections 36
4.3. Double viral injections in DG and CA3 38
5. Discussion 45
5.1. EC-DG connectivity 45
5.2. EC collateralization 48
6. Conclusion 54
7. References 56

List of Figures

- **Figure 1-1:** Diagram of the trisynaptic hippocampal loop
- **Figure 1-2:** Pattern separation in the hippocampus
- **Figure 1-3:** Pattern completion in the hippocampus
- **Figure 1-4:** Retrograde and anterograde labeling using static and transsynaptic tracers
- **Figure 3-1:** Methodology of transcardiac perfusion in rodents
- **Figure 4-1:** Viral tracing between the dentate gyrus and the entorhinal cortex
- **Figure 4-2:** Qualitative representation of rAAV2 labeling density
- **Figure 4-3:** Anterograde labeling of entorhinal cortex neurons and projections to the dentate gyrus
- **Figure 4-4:** Schematic representation of anterograde AAV injection into the EC and the proposed site of transport failure.
- **Figure 4.5:** Injection of HSV into layer II of the entorhinal cortex
- **Figure 4-6:** Hypothetical models of layer II EC neurons projections to the DG and CA3
- **Figure 4-7:** Retrograde viral circuit mapping of the entorhinal-hippocampal collateralized pathways
- **Figure 4-8:** Retrograde dextran collateralization between the EC-DG and EC-CA3
- **Figure 5:** Structural corroboration of EC projections to the DG and CA3

List of Tables

- Table 3-1: Coordinates of AAV injections in the Entorhinal Cortex
- Table 3-2: Coordinates of HSV injections in the Entorhinal Cortex
- Table 3-3: Coordinates of retrograde AAV injections in the Dentate Gyrus and CA3
- Table 3-4: Coordinates of retrograde dextran injections in the Dentate Gyrus and CA3

Abbreviations

- AAV – Adeno-Associated Virus
- AP – Anterior-Posterior (stereotaxic coordinate axis)
- AUUC – Animal Care and Use Committee
- BDA – Biotinylated Dextran Amine
- CA1 / CA2 / CA3 – *Cornu Ammonis* subfields 1, 2, and 3
- CMV – Cytomegalovirus (promoter)
- CTB – Cholera Toxin Subunit B
- DG – Dentate Gyrus
- DV – Dorso-Ventral (stereotaxic coordinate axis)
- EC – Entorhinal Cortex
- fMRI – Functional Magnetic Resonance Imaging
- GC / GCs – Granule Cell / Granule Cells
- GFP – Green Fluorescent Protein
- HSV – Herpes Simplex Virus
- KO – Knockout
- LEC – Lateral Entorhinal Cortex
- MEC – Medial Entorhinal Cortex
- MF / MFs – Mossy Fiber / Mossy Fibers
- ML – Medio-Lateral (stereotaxic coordinate axis)
- NGS – Normal Goat Serum
- NMDA – N-Methyl-D-Aspartate
- PBS – Phosphate-Buffered Saline
- PFA – Paraformaldehyde
- rAAV – Retrograde Adeno-Associated Virus (also AAVrg)
- TRITC – Tetramethylrhodamine Isothiocyanate

Abstract

The hippocampus, in conjunction with the entorhinal cortex, performs an indispensable function in the formation and retrieval of memories, thus rendering it one of the most extensively studied components of the brain, both in terms of function and structure. However, the quantification of these structural connections remains largely uncharted territory. Furthermore, there is a lack of insight regarding the parallel connections in the trisynaptic circuits. In light of these considerations, the objective was to ascertain the efficacy of various quantification methodologies in order to formulate a semi-quantitative approach to the number of connections between the entorhinal cortex and the dentate gyrus. In addition, the second objective was to ascertain the presence of any entorhinal cortex layer II neurons that project to both the dentate gyrus and CA3. In order to accomplish this objective, a combination of viral tracing and immunofluorescence techniques was utilised. It was determined through the application of these techniques that the quantification of entorhinal-dentate connections required tracers of a more refined nature than those employed in standard AAVs and pseudorabies viruses. Additionally, the confirmation was made that neurons within the entorhinal cortex project concurrently to both the dentate gyrus and CA3. These findings could assist in establishing a baseline for future investigations into the role of the hippocampus in pattern separation and completion, as well as the development of more precise computer models.

Acknowledgement

First and foremost, I would like to thank my supervisor, Dr. Katalin Tóth, for her guidance and unwavering support throughout this journey. I am also grateful to the members of my advisory committee for their insightful advice and constructive feedback over the course of our meetings. To my lab mates, thank you for your encouragement and support during the most stressful moments.

Finally, I owe my deepest gratitude to my family and friends, without whom I would not be where I am today. Everything I have accomplished is a reflection of their support and sacrifices. I am especially thankful to my mother and my sister, who have stood by me in my academic pursuits and in every other part of my life. No words can fully express how grateful I am to them, and how fortunate I feel to be part of this family.

1. Introduction

1.1. Entorhinal cortex

The entorhinal cortex (EC), otherwise referred to as Brodmann Area 28, is located within the medial temporal lobe. It is surrounded by the olfactory cortex, the amygdala, the parasubiculum, and the perirhinal cortex (Canto et al., 2008). As demonstrated in the relevant literature, it plays an important role in the integration of sensory information and is a major element of the hippocampal formation. This is essential for spatial navigation as well as memory processing and encoding (Basu & Siegelbaum, 2015; Witter et al., 2017). The EC facilitates communication between different cortical areas and the hippocampus by establishing connections between them. In the early 20th century, Santiago Ramon y Cajal produced a seminal work on the structure of the nervous system and the connections between neurons in different brain structures (Cajal, 1888; Lopez et al. 2007). His work provided insights that have guided most research regarding the brain's network and its functionality. In his illustrations, he delineated a structure within the posterior temporal cortex that exhibited a close association with the hippocampal formation, which was subsequently identified as the EC. This observation has led to a growing interest in the role of the EC in the transmission of information to the hippocampus and other cortical areas. It is now widely acknowledged that the EC is the primary source of input to and output from the hippocampal formation (Witter et al., 2017; Lavenex & Amaral, 2002). A number of studies have proposed a division of the EC into two distinct regions. As demonstrated in the seminal works of Blackstad (1956), Kerr et al. (2007), Witter (2007) and Van Groen et al. (2003), the medial entorhinal cortex (MEC) and the lateral entorhinal cortex (LEC) are the primary regions of interest in this field of research. By dividing the EC into two regions, researchers have been able to start explaining how different types of information are processed, thus facilitating a more in-depth understanding of the

differences in functions between LEC and MEC. The MEC and the LEC both project to the hippocampus. The layer II of the entorhinal cortex (EC) is composed of pyramidal and stellate cells, which are the primary source of projection to the dentate gyrus and CA3. The layer III of the EC is composed of pyramidal cells, which are the primary source of projection to the CA1 and subiculum. The MEC is located in close proximity to the hippocampus and is responsible for the processing of spatial information. The axons of these neurons extend towards granule cells and are located in the middle third of the molecular layer of the dentate gyrus. Within the MEC, there is also the presence of grid cells that fire in a hexagonal grid pattern, thereby providing a framework for understanding one's position within an environment. As demonstrated by Knierim et al. (2013), interaction between neurons and the hippocampal formation facilitates the retrieval of spatial memories, as well as their encoding. In contrast, the LEC is responsible for motivation and focus, and it extends its axons to the outer third of the DG' molecular layer. It has a dense network of connections with areas related to sensory processing and it is the principal structure related to associative and object memory by enabling the recognition and remembering of objects and their contextual associations (Knierim et al., 2014). The LEC is not as involved in spatial navigation, but it is nevertheless essential for contextualising memories (Save & Sargolini, 2017). For a considerable period, it was generally presumed that the level of connectivity of the human EC was analogous to that observed in rodents. This cross-species parallel was later confirmed by ultra-high-resolution fMRI, which facilitated the identification of a functional division of the human EC into two subregions. As demonstrated in the relevant literature, these areas exhibit distinct preferences for object-related recognition in the anterior-lateral subregion and spatial information in the posterior-medial subregion (Maass et al., 2015; Navarro Schröder et al., 2015; Schultz et al., 2015). Consequently, the functional architecture of the human EC is now recognised as a close

counterpart to the anatomical frameworks found in rodents and non-human primates (Mass and al., 2015). The existence of a correlation between two species can permit extrapolation from research findings on rodents to humans, albeit to a limited extent. However, despite the awareness of the origins of the projections for each structure, precise quantitative details, such as the exact number of connections each cell type in these regions' forms or if there is a redundancy in said projections, are lacking.

1.2. Hippocampus

The hippocampus is a complex structure of the brain located in the temporal lobe. The importance of this structure for the formation and retrieval of long-term memories related to specific individuals, locations, items and experiences has been extensively researched in rodent models. The hippocampus has the capacity to process multisensory information streams and collectively encode them as long-term memories. It is one of the only brain regions in which adult neurogenesis occurs, a process which is vital for learning (Bonfanti & Peretto, 2011). Some studies have also posited that said adult neurogenesis were one of the drivers of pattern separation, where young granule cells preferentially mediate pattern separation, while mature granule cells shift toward supporting pattern completion (Nakashiba et al., 2012). In the absence of the hippocampus, the ability to form new memories would be lost, as evidenced by the case of patient H.M. Following the removal of the majority of his hippocampus to treat his epileptic seizures, he was no longer able to form new memories and remained mentally stuck in 1953 for the remainder of his life (Penfield & Milner, 1958). The processes of memory recall and the formation of episodic memory require interactions between the dorsal hippocampus and the EC for the processing of multisensory information (Norman, 2010). The hippocampus is shaped like a seahorse and organised into three distinct parts: the dentate gyrus, the cornu ammonis, which is divided into three different subfields,

and the subiculum (Andersen et al., 1971). A distinctive property of the hippocampus that sets it apart from other regions of the brain is its predominant composition of unidirectional connections, forming a loop referred to as the trisynaptic circuit (Witter, 1993). The dentate gyrus is the recipient of inputs from the entorhinal cortex (EC) via the perforant path. These inputs are relayed by the dentate gyrus granule cells' axons, known as mossy fibres (MF), to the CA3 subfield. The CA3 subfield then relays the information to the CA2/CA1 complex via the Schaffer collaterals. Subsequent to processing, this input is then conveyed back to the entorhinal cortex via either the CA1 or the subiculum. It is also important to note that the EC connects directly to other regions of the hippocampus through different pathways.

1.2.1. Dentate Gyrus

The Dentate Gyrus (DG) is a fundamental cortical region of the hippocampal formation. It has been determined that the structure occupies approximately 25 to 30% of the volume of the hippocampal formation (Hagihara et al., 2009) and that its principal cell layers are arranged in a highly regular manner. It is the first structure in the hippocampus that receives input from the EC through the Perforant Path. The DG is divided into three layers. Firstly, the granule cell layer must be considered. It is composed of densely packed granule cells, with some neurons located at the boundary of the granule and polymorphic layers. The latter constitutes the second layer of the DG. Thirdly, the molecular layer is notable for its relative freedom from cells. It is composed primarily of the dendrites of the granule cells, in conjunction with the fibres of the perforant path, which have their origin in layer II of the EC (Amaral et al., 2008). Research employing paired recordings has demonstrated that a single granule cell can receive excitatory input from a group of EC cells, particularly in the region where the perforant path synapses with the dentate granule cells (Naughton et al., 1981; Hieber et al., 2004). As Leutgeb et al. (2007) demonstrate, upon receiving

inputs from the EC, the DG functions as a 'translator' between the cortical area and the rest of the hippocampal formation. This process involves the filtration of information received from the EC, and the subsequent conversion of dense cortical information into sparse hippocampal code. Subsequently, the MFs are projected to the CA3, where a significantly higher number of neurons are present, which facilitate the creation of distinct non-overlapping memories. In the rat brain, it has been established that layer II of the entorhinal cortex contains 120,000 principal cells that synapse with 1,200,000 granule cells. These granule cells, in turn, provide an input to 250,000 CA3 pyramidal cells (Arellano & Rakic, 2025; Rojas & Kreutz, 2016). The observed discrepancy in numerical values can be attributed to the low firing rate exhibited by granule cells, a property that has been demonstrated to enhance the probability of distinct granule cells encoding analogous inputs (Rojas & Kreutz, 2016). This ability to differentiate between similar experiences is a critical feature of episodic memory, and it is theorised that this ability drives the DG's capacity for pattern separation and completion in collaboration with the CA3 (Nakashiba et al., 2012; Bakker et al., 2008; Schmidt et al., 2011).

1.2.2. CA3

The CA3, in a manner similar to other regions of the hippocampus, fulfils a pivotal function in learning and memory consolidation. The CA3 neuron receives three principal excitatory inputs. The principal one is the mossy fibre input from DG granule cells. The mossy fibre pathway constitutes a significant unidirectional input from the DG, passing through the stratum lucidum and exhibiting large synapses on the proximal apical dendrites of CA3 pyramidal cells. It has been established that they are capable of inducing a significant depolarisation of CA3 neurons, thus resulting in the categorisation of MFs as conditional detonators (Kesner, 2013; Henze et al., 2002). In a manner comparable to the DG, the CA3 is also believed to receive input directly from Layer

II of the EC via the perforant path (Germtoth et al., 1989; Sammons et al., 2024; Sammons et al., 2025). This input could potentially serve as a recall cue, as suggested by Yassa & Stark (2011). A significant number of synapses within the hippocampus exhibit associative modification, as evidenced by the occurrence of long-term potentiation. This synaptic modification has been implicated in learning processes (Rolls, 2013; Nakashiba et al., 2009), and it has been theorised that the CA3 region exhibits a more complex internal connectivity compared to other regions of the hippocampus. CA3 pyramidal cells form an auto-associative network by ramifying and making excitatory contacts with neighbouring neurons (Lorente de Nó, 1934; Cherubini & Miles, 2015). This feature of the CA3 is hypothesised to drive pattern completion, where partial or degraded sensory input triggers the retrieval of a complete, stored memory representation. This phenomenon enables the brain to recall entire events from partial cues (Marr, 1971; Sammons et al., 2024).

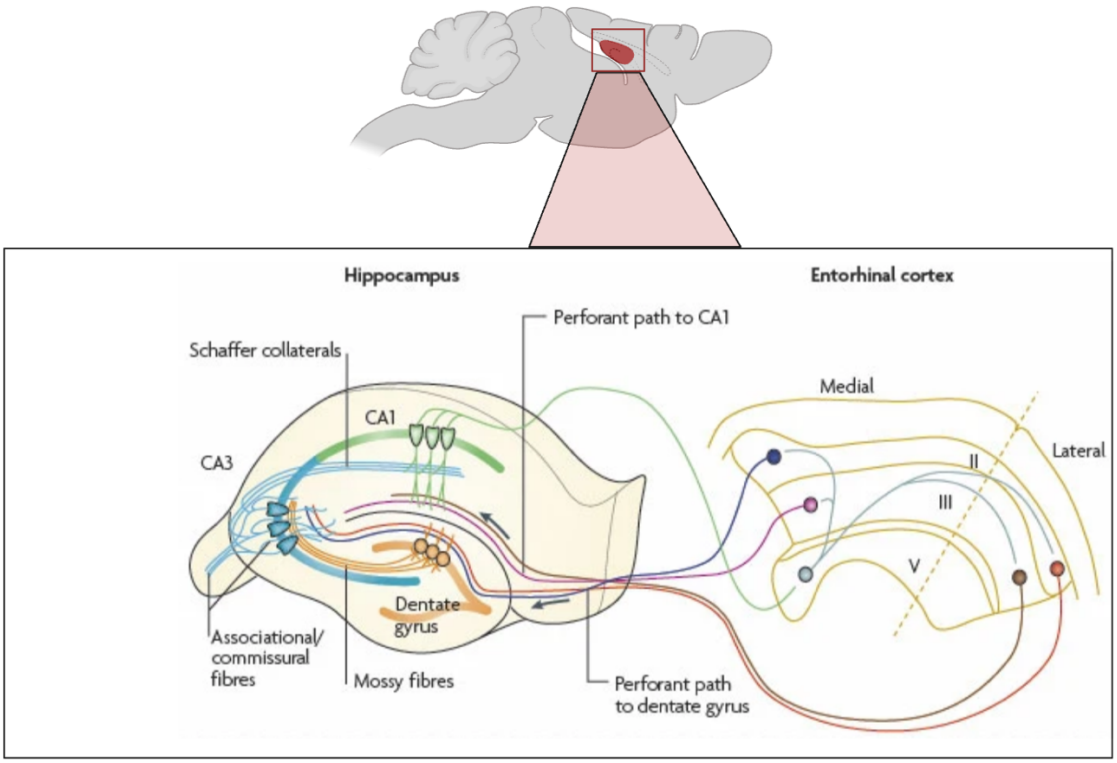


Figure 1-1: Diagram of the trisynaptic hippocampal loop. This figure represents the

organization of the hippocampal formation. This representation shows the major source input of the hippocampus, the entorhinal cortex where layer II neurons send excitatory axons through the perforant path to the molecular layer of the dentate gyrus. Those granule cells project to the CA3 through their mossy fibers and those innervated pyramidal cells make contact with the CA1 through the Schaffer collaterals. The CA3 also receives direct input from layer II entorhinal cortex cells through the perforant path and CA1 neurons receive direct input from layer III entorhinal cortex cells through the angular bundle. This figure was made with Biorender and adapted from Neves et al., 2008.

1.2.3. Pattern Separation

The concept of pattern separation, initially proposed by David Marr, facilitates the brain's ability to differentiate between similar experiences, thereby enabling the distinction between similar yet distinct memories (Marr, 1971). As posited by Norman and O'Reilly (2003), the hypothesis that pattern separation constitutes an essential parameter of episodic memory has been advanced. It has been theorised that the DG's granule cells possess the capacity to execute robust, domain-agnostic pattern separation, as evidenced by the proposal of several models. As previously mentioned, the DG accepts a dense input, such as the details of an individual's morning routine, and then expands it to encompass a much larger population of neurons. It has been demonstrated that overlapping representations in the EC would be transformed into non-overlapping representations in the DG. This transformation would then result in the projection of this distinct signal to the CA3. Despite the extensive research conducted on pattern separation in the hippocampus, it is crucial to acknowledge that this phenomenon does not exclusively depend on this particular brain region (Yassa & Stark, 2011). Furthermore, it has been evidenced that the DG was indispensable for spatial pattern separation. A study by Hunsaker et al. (2008) demonstrated that rats with lesions to the dentate gyrus (DG) exhibited an inability to discriminate between original and modified environmental conditions, thereby indicating an impairment in their pattern separation capabilities. At the receptor level, McHugh et al. (2007) demonstrated that selective deletion of N-methyl-D-aspartate (NMDA) receptors in mature granule cells induced a deficit in the mouse's ability to

discriminate between similar but different contexts during fear conditioning. In addition to the aforementioned studies, it has been demonstrated that the elimination of mossy cells present in the hilus results in a deficit in the discrimination of different contexts for fear conditioning, thereby revealing an impairment in pattern separation (Jinde et al., 2012). Pattern separation has also been the focus of human-based studies, in which it has been demonstrated that human hippocampal neurons possess the capacity to differentiate between overlapping representations through a photographic recognition test (Suthana et al., 2015).

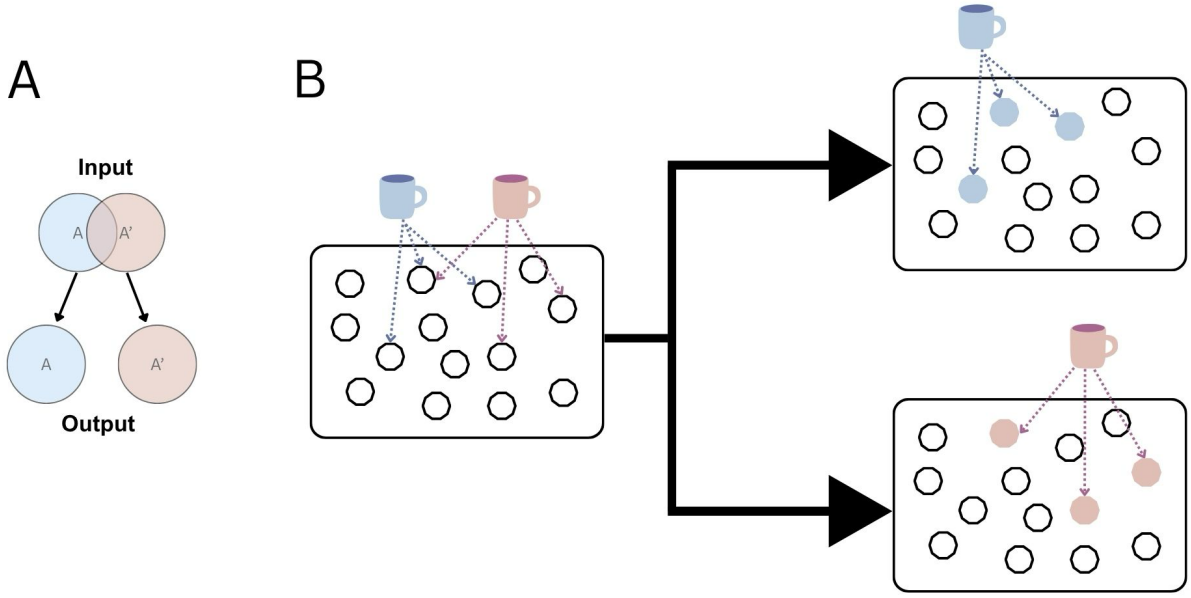


Figure 1-2: Pattern separation in the hippocampus. The figure represents overlapping inputs from the entorhinal cortex being coded separately by the dentate gyrus. A shows a conceptual representation of pattern separation whereas B shows two different contexts in the form of twodifferent colored mugs that are coded into two distinct neuronal fingerprints by the dentate gyrus. This image was created with Canva and adapted from Yassa et Stark, 2011 and from Lazarov et Hollands, 2015.

1.2.4. Pattern Completion

David Marr is also recognised for his seminal contributions to the field of cognitive neuroscience, particularly with regard to his pioneering work on the concept of recurrent collaterals and their

role in forming an auto-associative network that is capable of pattern completion. Pattern completion is defined as the process of reconstructing a complete memory from incomplete or degraded sensory data (Rolls, 2013). Therefore, while pattern separation is concerned with the maintenance of distinct entities, pattern completion pertains to the cognitive process of "filling in the blanks." The hypothesis that the MF pathway facilitates novel learning by imposing highly distinct pattern-separated representations on CA3 neurons to minimise interference and facilitate encoding was put forward on the basis of the direct collaterals that are sent to the CA3 by layer II EC neurons (Yassa & Stark, 2012). The direct EC-CA3 connection acts primarily as a cue to drive memory retrieval. Research has demonstrated that the lesions applied to the perforant path input to the CA3 region result in impaired retrieval, yet encoding remains unaffected. Conversely, the silencing of the MF pathway yields a contrasting outcome, with retrieval being intact while encoding becomes altered. The present findings indicate that the CA3 network integrates the training signal from the DG with the direct cue from the EC to facilitate subsequent recall (Kunec et al., 2005). Further evidence of pattern completion in the CA3 has been demonstrated in a number of studies. A study conducted using trained CA3-specific NMDA receptor knockout (KO) mice in a standard Morris water maze suggested that NMDA receptors within the CA3 are indispensable for pattern completion (Nakazawa et al., 2002). While the mutant mice demonstrated normal behaviour under conditions of full-cue availability, they exhibited substantial impairments in performance when partial environmental cues were absent. In a separate study, Gold and Kesner (2005) trained rats to locate concealed food items beneath objects by utilising four extra-maze cues. During baseline testing, the animals successfully retrieved the spatial locations even when less than all of the four cues were used, thus showing intact pattern completion. In contrast, rats that had sustained lesions in the CA3 region demonstrated a substantial decline in performance

when constrained to use only one or two clues. Consequently, it appears that the CA3 network is uniquely specialized for rapid, one-trial object-place recall and for pattern completion when triggered by incomplete retrieval cues.

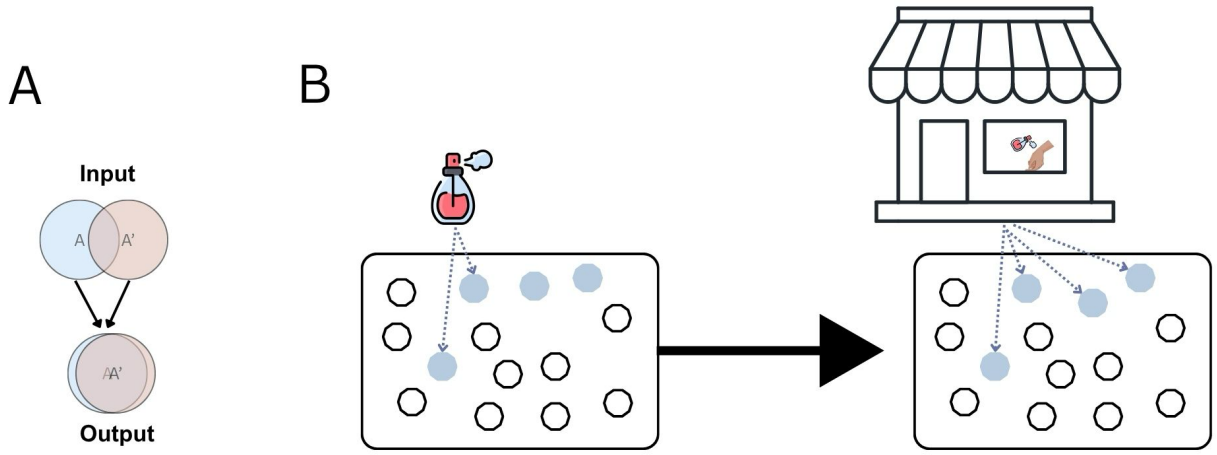


Figure 1-3: Pattern completion in the hippocampus. A represents a conceptual representation of pattern completion whereas B shows a partial subset of cue for context (Smell of perfume) that induces the retrieval of a whole memory (Remembering the moment you smelt the perfume for the first time at the store). This image created with Canva and adapted from Yassa et Stark, 2011 and from Lazarov et Hollands, 2015

1.3. Neuronal tracing

In the domain of neuroscience, neural tracing is a technique employed for the purpose of mapping structural connectivity within the brain. The employment of specific tracers facilitates the visualisation of neuronal pathways through the intracellular propagation of the tracer from the injection site to the connections that neurons in the area establish with other distant brain areas. In the early days of neuroscience research, scientists employed a range of methods to trace the

connections between neurons. One approach involved physically or electrically damaging a specific brain region, which resulted in the degeneration of the axons. This process rendered the axons uniquely susceptible to staining with silver, as documented by Fink et Heimer (1967) and Nauta (1952). Subsequent approaches were superseded by techniques that were based on axonal transport of injected materials from the injection site (Qiu et al., 2002). The categorisation of tracers is dependent upon the direction of their spread, which is to say that they are separated into two distinct categories. Anterograde tracers have been observed to disseminate from the cell bodies located at the injection site to the axonal region of the respective neurons. As demonstrated in the relevant literature, common anterograde tracers include adeno-associated viruses (AAV), biotinylated dextran amines (BDA), and plant lectins, amongst others (Zhao et al., 2017; Saleeba et al., 2019; Cuchiaro & Uhlrich, 1990). In contrast, retrograde tracers have been observed to disseminate from the axons located at the injection site to the soma of the target cells. Common retrograde tracers include cholera toxin subunit B (CTB) and pseudo-rabies viruses (Ericson and Blomqvist, 1988; Card & Enquist, 2014). In contemporary neuroscience, the employment of transneuronal vectors has become a prevalent method for the identification of neurons that are synaptically connected to one another. As Hui et al. (2022) describe, those tracers infect neurons in the targeted area and spread from that initially infected neuron to their directly connected neurons by jumping at the synapse between the two by exploiting the vesicular transport systems. In summary, upon infection of neuron A by the viral vector, the virus utilises vesicular machinery to travel to the synapse, subsequently entering neuron B via endocytosis at the synapse. The ability of these tracers to cross synapses is specifically advantageous for the purpose of molecular precision, thereby facilitating the imaging of long-distance or complex connections with high resolution (Ohara & Iijima, 2009).

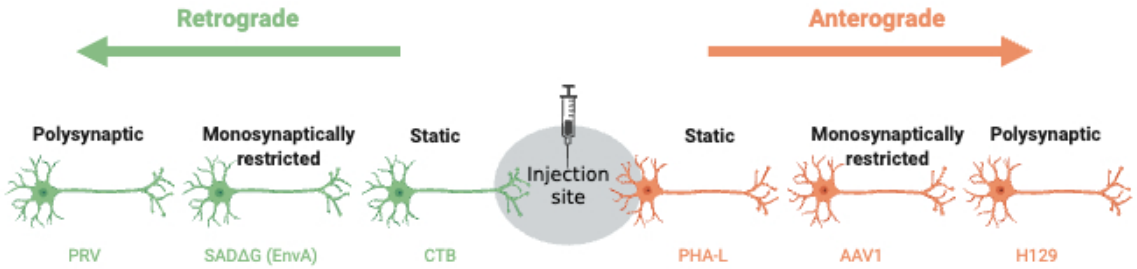


Figure 1-4: Retrograde and Anterograde labeling using static and transsynaptic tracers. This figure depicts the different categories of tracers based on their direction and level of travel within neurons. Retrograde tracers are taken up by axon terminal and travel to the cell body while anterograde tracers are taken up by cell bodies and travel to axons terminals. There is also a representation of different type of tracers, static tracers staying strictly within the infected neurons whereas monosynaptic and polysynaptic tracers can spread transsynaptically respectively to one or more neurons. This figure was created with Biorender and adapted from Saleeba et al., 2019.

2. Objective and Significance

2.1. Quantification methods between Entorhinal Cortex and Dentate Gyrus

The connectivity between EC and DG cells involves both direct and indirect pathways, where multiple EC cells converge onto a single DG granule cell, and there is a high degree of convergence (Cholvin and Bartos, 2026). Despite the existence of substantial qualitative research regarding the structures of the EC and DG, a notable gap remains concerning the quantitative nature of the synaptic connections between these two structures. As Amaral et al. (1990) rightly asserted: "There is an absence of direct anatomical evidence regarding the total number of synapses that each entorhinal neuron contributes to the dentate gyrus, or whether an entorhinal cell makes 1, 100, or 1000 synapses on a single dentate granule cell. The population-level picture has since been revised substantially, but not through direct measurement of single-cell connectivity. Design-based stereology has recalculated the estimated number of layer II neurons in the rat (Arellano & Rakic, 2026), and electron microscopy of granule cell dendrites has roughly estimated number of the excitatory synapses per granule (Popov & Stewart, 2009; Thind et al.,2010; Bromer et al., 2018).

Furthermore, there is a notable absence of information regarding the total number of inputs received by a single hippocampal neuron. The precise number of EC cells that connect to a single DG granule cell is subject to variation, contingent on the specific region of the dentate gyrus under consideration (for instance, the outer versus inner molecular layer) and the functional characteristics of the implicated cells. Researchers have been able to target dentate gyrus cells sparsely in order to observe the intensity of labelling in different layers of the entorhinal cortex. Conversely, an anterograde virus has been injected into the entorhinal cortex, enabling the observation of the density of labelling in each layer of the dentate gyrus. However, to date, no studies have been conducted that have accurately measured the number of these connections. Therefore, it is evident that this information would be of crucial importance. The existence of a quantitative measure of these connections could assist in the development of future studies, including the construction of computational models. These models could enhance our comprehension of signal propagation, as well as synaptic strengths and mechanisms. In light of the aforementioned points, the following two questions were raised for consideration: How many EC cells connect to one DG cell? How many DG cells does one EC cell connect to? Furthermore, it may be possible to enhance our understanding of each EC cell's function in disseminating information throughout the hippocampus and facilitating the development of adaptable, dispersed memory traces by determining the extent of its projections within the DG. By ascertaining this number, researchers can gain insight into the propagation and scaling of input signals through the hippocampal circuitry and assess how a single input can lead to widespread or selective memory encoding. Therefore, ascertaining the extent of convergence and divergence between these two structures is imperative for understanding how information from disparate sources is integrated within the hippocampal formation. That understanding would also facilitate the development of

targeted solutions for neurodegenerative diseases in the future. The objective of this research is to establish a benchmark for the techniques demonstrating the highest potential for addressing the question of quantitatively estimating those connections. This will be achieved by using a combination of different transsynaptic and static tracings through stereotaxic injections and confocal imaging.

2.2. Collateral connectivity of Layer II Entorhinal neurons

The second objective of this thesis was to determine whether individual EC layer II neurons could send collateral projections to both the DG and CA3 simultaneously. As demonstrated in previous anatomical studies, EC projections to the CA3 and the DG are predominantly located in layer II. However, the question of whether single neurons project to both targets remains unresolved (Witter et al., 1989; Tamamaki & Nojyo, 1993). The employment of this dual-labelling approach resulted in the identification of double-labelled EC neurons, thereby enabling the direct addressing of the research question in a manner that was both time-efficient and technically reliable. The identification of dual-projecting EC neurons has the potential to provide insights into the coordination of upstream cortical information across these computationally distinct subcircuits. In the event of a subset of layer II EC neurons being double labelled, this would provide strong evidence that individual EC neurons collateralise to both DG and CA3. This finding would imply that specific EC neurons distribute the same cortical input into both the trisynaptic and monosynaptic pathways. This outcome would have significant implications for understanding information processing in the hippocampus, indicating that some neurons may broadcast identical signals to regions responsible for pattern separation and pattern completion. If neurons with specific labels are found to form two non-overlapping populations, this would indicate that EC input to DG and CA3 arises from anatomically distinct neuronal pools. This outcome would lend

further support to the hypothesis that the hippocampal subcircuits receive segregated streams of cortical information. The interpretation of EC functional heterogeneity would be enhanced by such data, which could provide a framework for understanding differential vulnerability across hippocampal pathways in disease models.

3. Methods

3.1. Animals

The experimental subjects were C57BL/6 mice (Coat Color: Black, MHC Haplotype H2b, Strain Code: 027) that were between 2 and 4 months of age. In all experiments, subjects of both sexes within the same age group were included. The mice were fed a standard diet and provided with unrestricted access to water. The experimental subjects were maintained under a 12:12 light:dark cycle in a climate-controlled facility. All animal care and experimentation adhered to the guidelines established by the Animal Care and Use Committee (ACUC).

3.2. Stereotaxic Injection

Stereotaxic surgery is a high precision technique used to target specific brain areas using a three-dimensional coordinate system from a set reference. In this particular instance, the point of reference is Bregma, which is defined as the point on the skull where the coronal and sagittal sutures meet. An hour prior to surgery, the mice received a subcutaneous injection of SR-Buprenorphine (1.2 mg/kg). Subsequently, the mice were anaesthetised using 4% isoflurane for a period of 3-5 minutes. After ensuring the mice were fully anesthetized by pinching their foot, they were then positioned on the prep station under continuous anaesthesia. The mice were then

subjected to a hair removal procedure using an electric razor, and the shaved area was meticulously disinfected using a combination of ethanol and iodine. Subsequently, the mice were head-fixed on a stereotaxic frame and anaesthetised continuously using 2.7% isoflurane. Bupivacaine (2 mg/kg) was injected subcutaneously into the mouse skull. Following this, a small incision was made on the head to expose the skull, with the landmarks of bregma and lambda being exposed. Following the determination of the appropriate coordinates, the injection was administered through the drilling of a small hole in the skull at the corresponding coordinates, thereby exposing the surface of the brain. The following procedure was then carried out: a glass pipette was backfilled with mineral oil containing the tracer and then lowered at the targeted site. The injection was then performed using a Drummond pump. After undergoing the surgical procedure, the mice were administered 1 mL of saline and transferred to a new cage.

3.3. Perfusion

Following the stereotaxic injections, a designated waiting period was allocated for each tracer, with the objective of ensuring sufficient time for the them to travel. This period of incubation is of critical importance in ensuring that the tracers have sufficient time to infect the neurons and propagate along their axons, thus facilitating effective tracking of the connections between these two brain regions. The waiting period also allows for any viral tracer to make at least one synaptic jump, moving from the neuron initially infected by the virus to downstream neurons that form synaptic connections. After this period, the mice were transcardiacally perfused with 4% paraformaldehyde (PFA) (see Figure 3-1). Following perfusion, the mice were decapitated, and their brains were collected and post-fixed overnight in PFA. Perfusion with PFA is a critical step in preserving brain tissue and preventing post-mortem changes. This method ensures that the fixative is able to penetrate the brain quickly and evenly, which is a more challenging feat to

accomplish with post fixation. Indeed, post-fixation does not prevent the initial stages of autolysis, meaning that certain structures may degrade before fixation takes effect. Therefore, the process of perfusion with PFA is an effective method of rapidly halting the degradation processes that occur within the tissue. The effect of this treatment is to stabilise the cellular structures and to preserve the tissue in a state that closely resembles its living state. This is of paramount importance for the subsequent steps of tissue sectioning and high-resolution imaging, both of which are integral to the success of this project.

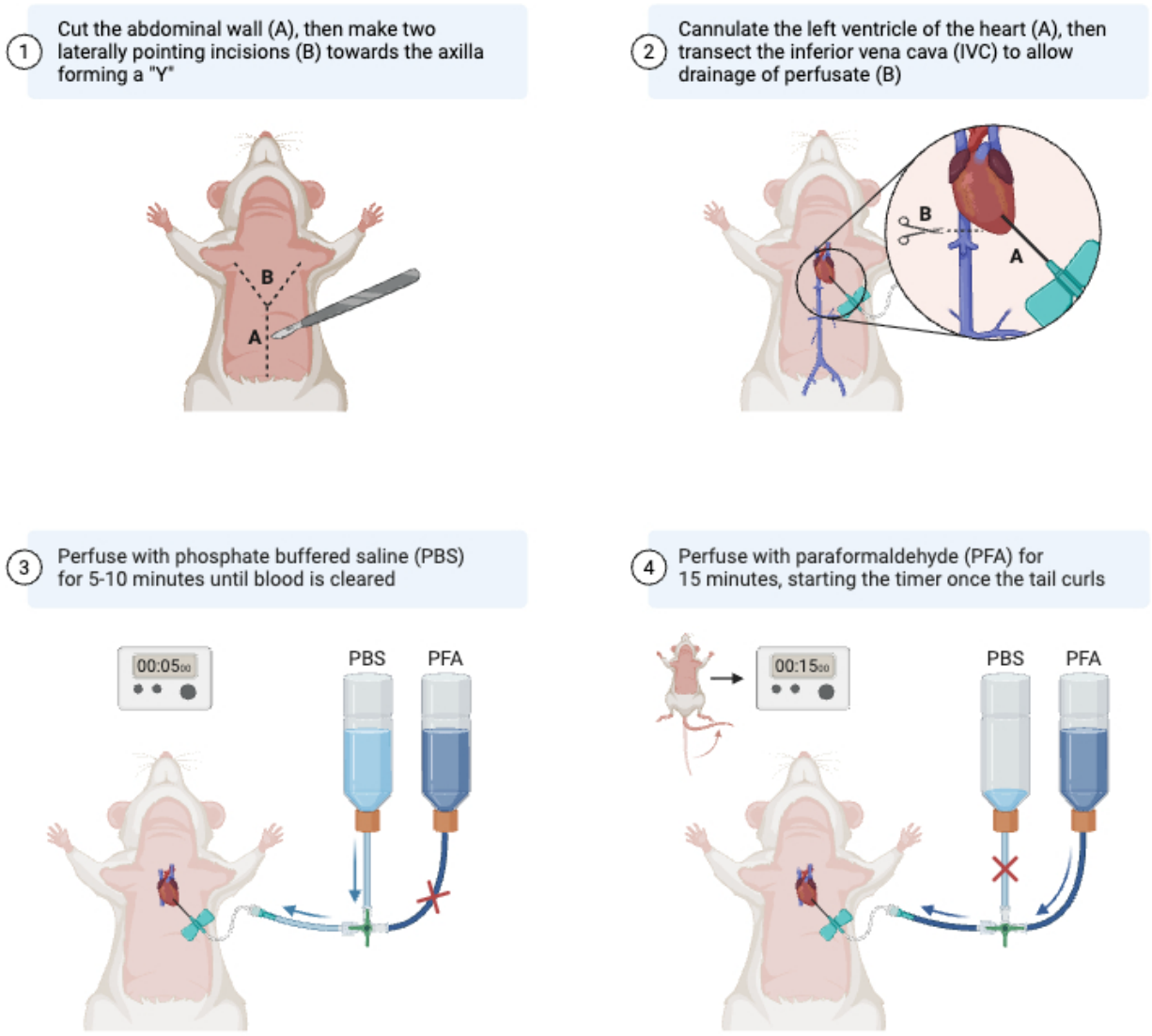


Figure 3-1: Methodology of transcardiac perfusion in rodents. Made with Biorender

3.4. Anterograde tracing

In order to trace the number of granule cells that connect to one EC cell, anterograde transsynaptic tracing was employed. This technique utilises a tracer, in this case a viral vector, which is injected into a specific brain region and subsequently travels across synapses. By tracking the movement of the virus across synapses, it is possible to approximate the number of EC cells connected to a single DG cell, and vice versa. In selecting the most appropriate viral vector, a multifaceted evaluation process was employed, encompassing considerations such as tropism, infectivity, and toxicity. In consideration of the aforementioned factors, our research was directed towards Adeno-Associated Viruses (AAVs). The rationale for this decision was that AAVs offer several advantages in this particular context, including their minimal immunogenicity, lack of toxicity, and the capacity for sustained expression over a period of several months. In this case, the virus will be taken up by EC neurons and anterogradely transported to their post-synaptic partners in the DG. Consequently, by injecting the AAV into the EC, it is possible to quantify the number of cells that have been labelled in the EC and the number of cells that have acquired the virus from the synapse jump in the DG. This allows us to determine the average number of connections between one EC cell and an X number of DG cells. For instance, if following injection of the AAV into the EC, one cell is labelled and subsequent imaging reveals that ten granule cells are labelled, then it is possible to make a rough estimation that ten granule cells are contacted by a single EC cell. The gene that is responsible for the production of green fluorescent protein (GFP) is expressed by the virus, facilitating its visualisation. This is due to the fact that infected cells express GFP, thus enabling the tracking of the distribution and propagation of the virus. The injections targeted layer II of the EC, as this layer is the primary source of projections to the DG. Two distinct sets of coordinates

were used to target the second layer of both LEC and MEC (see Table 3-1). The objective of this injection was to quantify the number of DG cells that would take up the virus in comparison to the labelled EC cell, and to approximate the number of granule cells that are connected to one EC cell. The objective was to minimise the labelling, with the intention of targeting approximately ten to fifteen EC cells in order to track their projections to the DG, thus enabling the quantification of an average number of those projections.

Structure	AP	ML	DV	Vectors injected	Original titer (vg/mL)	Volume injected (nL)
LEC	-4.16	+/-3.75	-4.20	pAAV-CMV-GFP	1×10^{13}	25-100
MEC	-4.50	+/-3.20	-4.40	pAAV-CMV-GFP	1×10^{13}	25-100

Table 3-1: Coordinates of AAV injections in the Entorhinal Cortex. Summary of coordinates of injections relative to Bregma and indications of the vectors injected as well as their titers and volumes. pAAV-CMV-GFP (CAT: D3312, LOT: 2983200)

Additionally, we employed the Herpes Simplex Virus (HSV) for the anterograde tracing procedure due to its ability to facilitate a more expeditious infection rate and a known temporal spread, despite the fact that it carries a higher risk of inflammation at the injection site. HSV is exclusively anterograde, with a larger packaging capacity compared to AAVs, which could prove advantageous for enhancing cell-type specificity by accommodating larger genetic payloads (Wojaczynski et al., 2015). The injections targeted the same locations for both MEC and LEC, and the quantitative cell target goal remained unchanged (see Table 3-2).

Structure	AP	ML	DV	Vectors injected	Original titer (pFU/mL)	Volume injected (nL)

LEC	-4.16	+/-3.75	-4.20	HSV (H129)	7.38^{9}	10-25
MEC	-4.50	+/-3.20	-4.40	HSV (H129)	7.38^{9}	10-25

Table 3-2: Coordinates of HSV injections in the Entorhinal Cortex. Summary of coordinates of injections relative to Bregma and indications of the vectors injected as well as their titers and volumes. HSV (H129, #772)

3.5. Retrograde tracing

3.5.1. Monosynaptic AAV mapping

In order to trace the number of EC cells that connect to a single DG cell, the following procedure was undertaken. Firstly, a retrograde AAV (Tervo et al., 2016) encoding green fluorescent protein (rAAV-CAG-GFP) obtained from Addgene was injected into the DG of wild type mice. The aliquots were stored at -80°C and thawed on ice immediately prior to injection. The total volume of solution injected into the dentate gyrus was between 50 and 100 nanolitres. The injections were targeted to the following coordinates from bregma: AP = -2mm, ML = ±1.25mm, and DV = -2mm.

3.5.2. Monosynaptic viral double-labeling

In order to investigate the collateralisation of EC projection neurons to both the DG and the CA3 region, dual retrograde viral tracing was performed. The delivery of two separate fluorophores into the DG and CA3, respectively, enables the identification of individual neurons projecting to both targets via the co-expression of both fluorescent proteins. In order to target the DG injection, an injection of AAV-retro-CAG-GFP (Addgene, CAT: 37825-AAVrg) was made, with the aim of targeting the molecular/granule cell layer in order to label the perforant path projection axons originating from layer II of the EC. In the CA3, we injected AAV-retro-CAG-mCherry targeted to the pyramidal cell layer of the CA3 to label the perforant input pathway (see Table 3-3).

Structure	AP	ML	DV	Vector injected	Titer	Volume injected (nL)
DG	-2.00	+/-1.25	-2.00	rAAV-CAG-GFP	7×10^{12}	50
CA3	-2.30	+/-2.5	-2.40	rAAV-CAG-mCherry	7×10^{12}	50

Table 3-3: Coordinates of retrograde AAV injections in the Dentate Gyrus and CA3. Summary of coordinates of injections relative to Bregma and indications of the vectors injected as well as their titers and volumes.

3.5.3. Monosynaptic non-viral double labelling

To independently validate the collateralisation patterns that were observed with the viral tracers, a secondary technique of dual retrograde tracing was used in the form of hydrophilic dextran amines. Dextrans are considered to be an excellent method of validation due to their passive retrograde transport and distinct chemical properties, thus eliminating potential biases related to tropism or promoter-dependent gene expression. In this instance, two fluorescently conjugated dextrans were injected into the DG and the CA3. The DG was targeted with an Alexa Fluor 488 dextran (Thermofisher), and the CA3 was targeted with Miniruby, which is a biotin-conjugated dextran amine (BDA). The stereotaxic coordinates corresponded to those employed for the viral injections, in order to visualize double labeled neurons in the EC (see Table 3-4).

Structure	AP	ML	DV	Vector injected	Molecular Weight	Volume injected (nL)
DG	-2.00	+/-1.25	-2.00	Alexa 488 Dextran	10000	50 nL
CA3	-2.30	+/-2.5	-2.40	Miniruby Dextran	10000	50 nL

Table 3-4: Coordinates of retrograde dextran injections in the Dentate Gyrus and CA3. Summary of coordinates of injections relative to Bregma and indications of the vectors injected as well as their molecular weights and volumes.

3.6. Slicing

3.6.1. Vibratome

Following post-fixation, the brain will be prepared for histological analysis by slicing. The fixed brains were embedded in 4% agar to provide structural support during sectioning, thereby preventing tissue distortion and preserving the integrity of brain structures. Subsequent to the complete solidification of the agar, the block was trimmed and secured to the specimen stage of a vibratome. The buffer tray was filled with Phosphate Buffered Saline (PBS) to ensure optimal cutting conditions. The brains were then sectioned coronally at a thickness of 50-micron sections. The sections were then collected free floating in 24 well plates that had been filled with PBS. The plates were then stored at a temperature of 4°C, pending the next stage of the histological processing.

3.6.2. Microtome

Prior to sectioning, the tissue was cryoprotected by means of immersion in a 30% sucrose solution in 1xPBS at 4° until fully saturated. For the purpose of sectioning, the brains were mounted onto the specimen stage of a freezing microtome using a thin layer of water. The brains were then stabilized by being covered with crushed dry ice in order to ensure rapid, uniform freezing. The brains were then sectioned at a thickness of 35 microns, and the resulting free-floating sections were collected in 24-well plates filled with 1xPBS.

3.7. Immunofluorescence

In instances where the viral signal was inadequate for clear visualisation, immunofluorescence was employed to enhance the detection of the tracer. The slices were initially washed thrice for 10 minutes each in 0.1M PBS (pH 7.4) at room temperature in order to remove any excess fixative.

Thereafter, the tissue was permeabilised in 0.5% Triton X-100 in PBS for a period of 30 minutes at room temperature. Permeabilization is a pivotal stage in the process, as it allows for the successful penetration of the antibody into the slices. Following permeabilization, the wash step was repeated three times for 10 minutes in PBS. Non-specific binding sites were then blocked by incubating the sections in 10% Normal Goat Serum (NGS) diluted in PBS for a period of 60 minutes at room temperature. For the immunolabeling procedure, the slices were incubated in the primary antibody, which had been diluted in PBS containing 1% NGS. The incubation process was conducted overnight at a temperature of 4°C. Subsequent to this, the slices were subjected to a series of washes, with each wash consisting of 10 minutes of immersion in PBS at room temperature. The slices were then subjected to an incubation process with a secondary fluorophore-conjugated antibody, which had been previously diluted in PBS solution. This incubation process was carried out for a period of six hours at room temperature. Following a series of three final washes for a duration of 10 minutes in PBS, the sections were meticulously mounted onto glass slides using Fluoromount G mounting medium (Invitrogen, Cat. No. 00-4958-02). The slides were then cover slipped for the purpose of fluorescence imaging.

3.8. Imaging

The slides were imaged using a confocal microscope which facilitates the acquisition of high-resolution, three-dimensional imaging of brain tissue. The confocal system facilitates the analysis of the distribution of tracers by enabling the tracking of specific layers within the tissue (Z stack). This in turn provides insight into the synaptic connections between the entorhinal cortex and the hippocampus, by evaluating the spread of the tracers from the former to the latter. Therefore, an analysis was conducted on the acquired images in order to quantify the synaptic connections

identified between the entorhinal cortex and the dentate gyrus, as well as the CA3. In order to locate the EC and the hippocampus, the sections were first scanned at low magnification (10X). The EC was identified based on anatomical landmarks such as the rhinal fissure and the laminar organisation of its layers, and the hippocampus was identified by its characteristic shape. For the purpose of high-resolution mapping, the images were acquired using a higher magnification objective. The excitation of green fluorescent protein (GFP) fluorescence was accomplished through the utilisation of a 488-nm laser line, while the excitation of mCherry and Miniruby was achieved by employing a 546-nm laser line.

4. Results

A comprehensive understanding of the number of EC cells that synapse onto a single DG cell would provide significant insights into the processing and pooling of sensory data prior to its entry into the hippocampus network. The quantification of this number could elucidate the manner in which diverse inputs are integrated and transformed within the dentate gyrus, thereby enhancing our understanding of its role in spatial and episodic memory formation as well as pattern separation. This prompted the following inquiries: Which direction of the EC-DG pathway should be investigated in order to conduct quantification experiments? Which type of viral tracer would be the most suitable for each of these routes? In order to address these questions, a decision was taken to conduct an investigation into both the retrograde and the anterograde route, making use of a number of tracers.

4.1. Retrograde AAV tracers allowing for sparse labeling of GCs in the DG

The objective of this study was to ascertain the efficacy of employing viral tracers to label DG neurons and to determine the number of their presynaptic partners in the EC. Retrograde AAVs have been demonstrated to be reliable tracers for hippocampus labelling in previous studies.

However, it has been observed that this labelling is frequently accompanied by direct viral uptake by EC cells. This indicated that the investigation of the numerical connectivity between EC and DG via the retrograde route might not be possible. This prompted an investigation into the feasibility of labelling granule cells without concomitant labelling of EC cells axons. The aim of the retrograde experiments was then to count the entorhinal neurons that synapse onto a single granule cell. Two events were expected. First, direct infection of a few granule cells at the injection site, which serve as starter cells. Second, uptake of virus by entorhinal axon terminals in the injected volume and retrograde transport to their somata, as described by Tervo et al. (2016) for projection neurons. Three outcomes were possible. (A) Granule cells labelled, and no entorhinal neurons labelled. (B) Granule cells and entorhinal layer II neurons labelled. (C) Entorhinal labelling restricted to neurons that contact the labelled granule cells. We therefore examined whether dose and volume could be tuned so that granule cells were labelled sparsely while terminal uptake by entorhinal axons fell below detection. To this end, a retrograde AAV was used to label DG neurons by performing a stereotaxic injection in the DG, as previously described. The objective of the procedure was to administer the precise volume and concentration of virus to obtain sparse labelling and to prevent bleed through to the EC's axons located in the molecular layer. In order to accomplish that objective, it was decided that multiple viral volumes and concentrations would be tested. Following the administration of injections (n=4), it was determined that at elevated concentrations, such as 7×10^{13} vg/mL, the minimum volume that could be injected (10 nL) resulted in the formation of excessively dense clusters of labelled GCs (Figure 4-1-A). A broad fluorescent signal was observed in the DG, with the diffusion pattern indicating a significant localised expression. It is evident that the EC was also labelled with clusters of cells, which is indicative of the fact that EC's axons picked up the virus through the molecular layer.

This clustering precluded the accurate quantification of the cells that were labelled, as it was not possible to obtain a clear view of individual neurons, nor their arborisations, for the purpose of counting them.

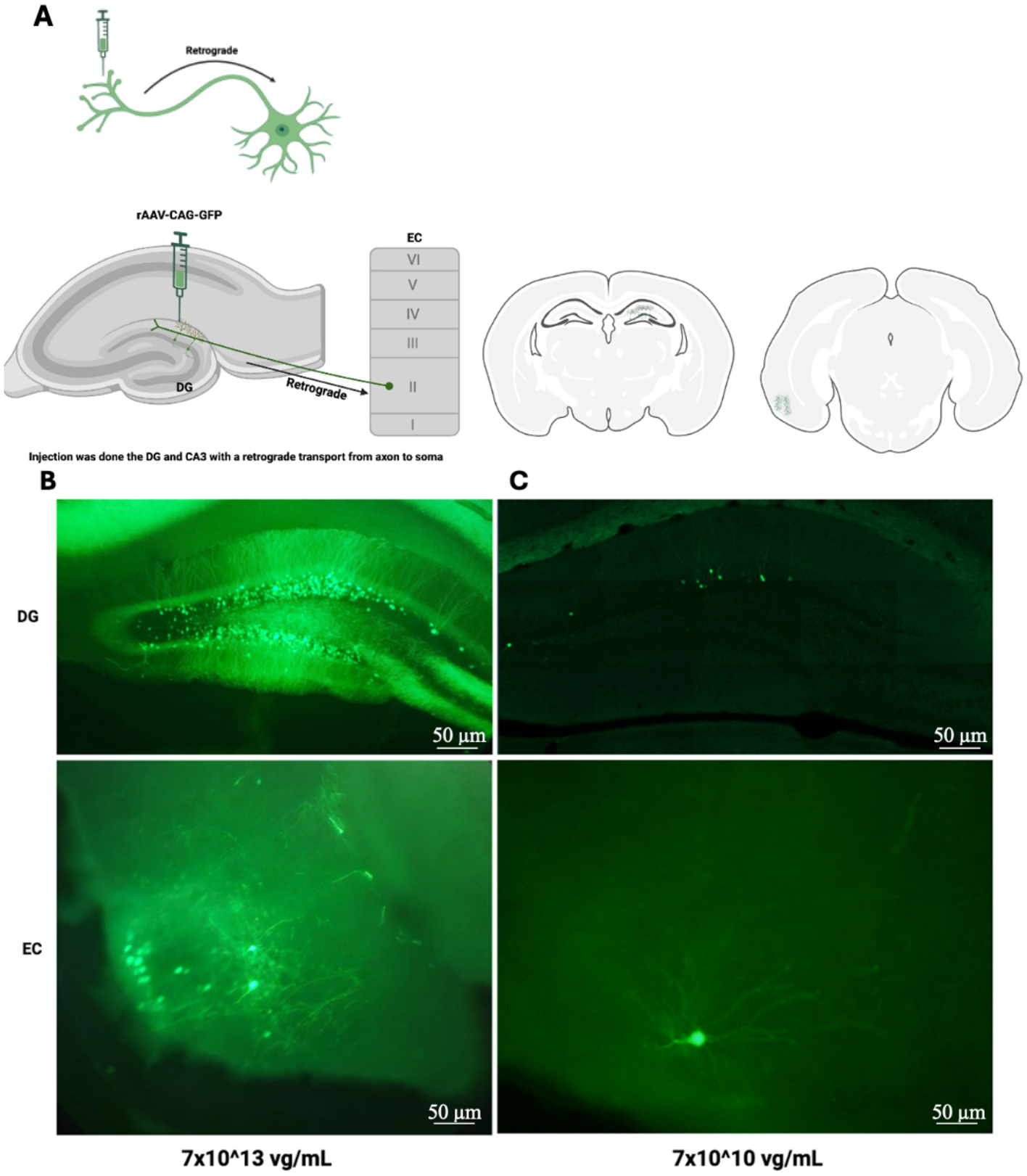


Figure 4-1: Viral tracing between the dentate gyrus and the entorhinal cortex. A. Shows the

injected structure and the retrograde direction of travel of the virus as well as its coronal representation. **B.** The top panel shows a broad fluorescent signal in the DG. The diffusion pattern suggests a strong localized expression with some spread along the molecular layer. The right panel shows labeled neurons in the entorhinal cortex, indicating that the viral tracer has also labeled some presynaptic EC cells. The fluorescence signal reveals multiple labeled neurons with visible axons and dendritic arborizations. **C.** The top panel presents a clearer view of individual neurons within the DG, some labeled neurons can be seen with their dendritic arbor extending into the molecular layer. The fluorescence intensity is lower than in the first in order to distinguish individual neuronal structures, including soma and initial dendritic processes. The bottom panel shows for the same mouse a labeled EC cell representative of a viral uptake by the EC. (Made with Biorender)

The abundance of labeling prompted us to reflect on two fundamental questions: 1) Would dilution result in the reduction of cell clusters to a countable number? 2) Is the targeted surface area, the cause of direct labelling of the EC? The aim was then to systematically dilute the virus in order to label a smaller neuronal population in the DG with cells that would be easy to differentiate and clear processes. Subsequently, a series of concentrations were examined, ranging from $7x10^{12}$ vg/mL to $7x10^{8}$ vg/mL, with two mice injected for each concentration. It was observed that with each dilution, there was a decrease in the number of clusters. (Figure 4-1-B). It was also established that the optimal sparse labeling was achieved with concentrations of $7x10^{9}$ vg/mL and 7×10^{10} vg/mL. After tissue processing, we would typically identify two to four granule cells present in the DG with a clear view of each individual neuron within the DG and with a distinguishable neuronal structure including soma and initial dendritic processes with their dendritic arbor extending into the molecular layer. The sparse labeling obtained suggested a correlation between the concentration and the quantity of cells labeled. However, the dilution only solved the question about density of the label but not the spread of the virus which still left the question of direct label. That brought us to question if by reducing the volume, it would be possible to contain the viral spread enough not to label the EC by direct uptake.

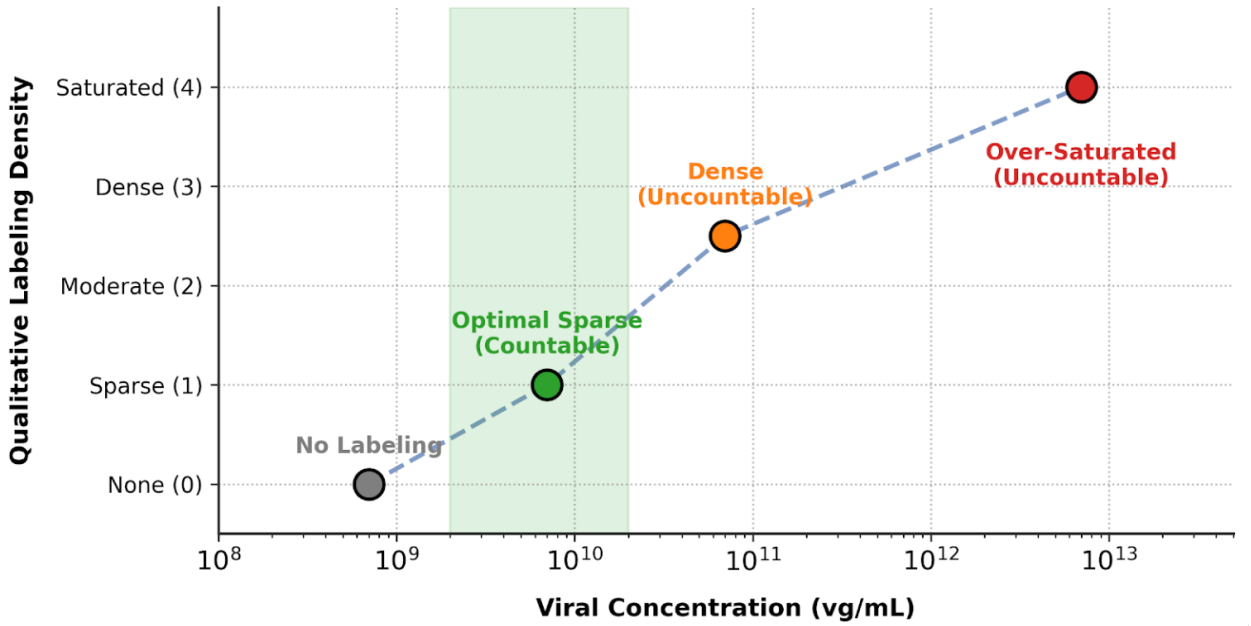


Figure 4-2: Qualitative representation of rAAV2 labeling density. The density of transduction between $7x10^9$ and $7x10^{10}$vg/mL shows an optimal operational window where the transduction is low enough to ensure a sparse labeling of granule cells. Below that window, no signal was detected providing no quantifiable data. Above that window, the density of labeled cells grows drastically resulting in an over-saturated expression of GFP+ granule cells.

In order to investigate the role of volume in containing the spread in a way that it would not reach EC axons, different injections were performed. Each time, the volume of virus injected at the optimal concentration was reduced. This concentration had been determined in previous trials to be between 7×10^9 vg/mL and 7×10^{10} vg/mL (see Figure 4-2). The injection volumes employed in this study ranged from 5nL to 300nL. Following a series of trials, it was determined that injections of 50 nL at concentrations of approximately 7×10^{10} vg/mL resulted in adequate sparse labelling of the DG, rendering it quantifiable. However, at these low concentrations, small labelling of EC neurons was still observed, indicating a viral uptake from EC axons (Figure 4-1-B). The presence of labelled EC cells indicates that a bias in quantification would be introduced by the use of a regular retrograde transsynaptic tracer, as it would not be possible to ascertain whether the labelled EC neurons were actually connected to the granule cells that had been labelled in the dentate gyrus,

or whether it was merely the result of EC neurons acquiring the virus independently. This would thus convolute our quantification and would give us a wrong approximation of the number of connections if we were to use that method. Because EC cell labelling persisted even at the optimal injection volume (50 nL) and titre (7 x 10^{10} vg/mL), direct retrograde quantification of EC to DG connectivity via standard retrograde AAVs was deemed to be unviable. This persistent limitation introduced an unresolvable bias for numerical connectivity analysis, prompting a shift in the investigation towards the anterograde route to assess whether tracing from the EC to the DG would solve the direct uptake problem.

4.2. Injections in the entorhinal cortex

4.2.1 AAV anterogradely travel from the EC but fail to cross synapse in DG

In order to evaluate the potential of anterograde adeno-associated virus (AAV1) tracing for systematic quantification of the number of EC neurons that synapse onto individual granule cells, the initial objective was to assess the performance of the virus. In this structural network analysis, the tracing technique used was intended to differentiate between different variables. Firstly, it was used to determine whether there was actual transsynaptic transduction instead of an extracellular diffusion or passive leakage. Secondly, it was used to determine whether the absence of signal was due to the pathway lacking the right machinery for the virus to cross the synapse.

The initial injection of AAV1 at a high concentration of 1x10^{13} vg/mL facilitated the establishment of a baseline; however, it also exposed significant quantitative obstacles. At the injection site in the EC, dense fluorescent somatic clusters were observed, resulting in an inability to accurately separate or count individual cells (see Figure 4-3-A). The heavy labelling of axons in the molecular

layer confirmed the capacity of the virus to travel anterogradely through the machinery down the perforant path. However, the absence of labelled granule cells revealed the inability of the virus to cross the perforant path synapse, despite reaching axon terminals.

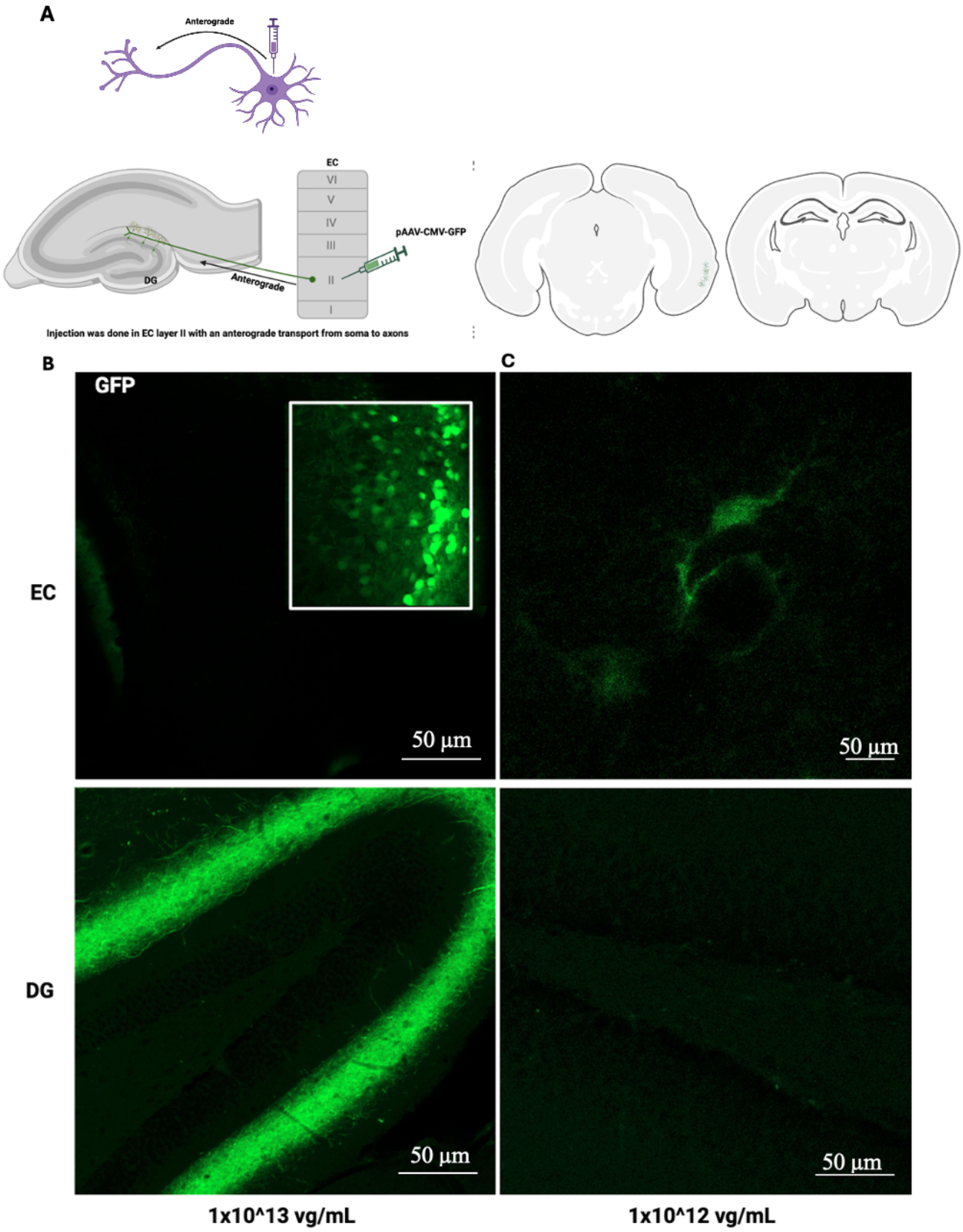
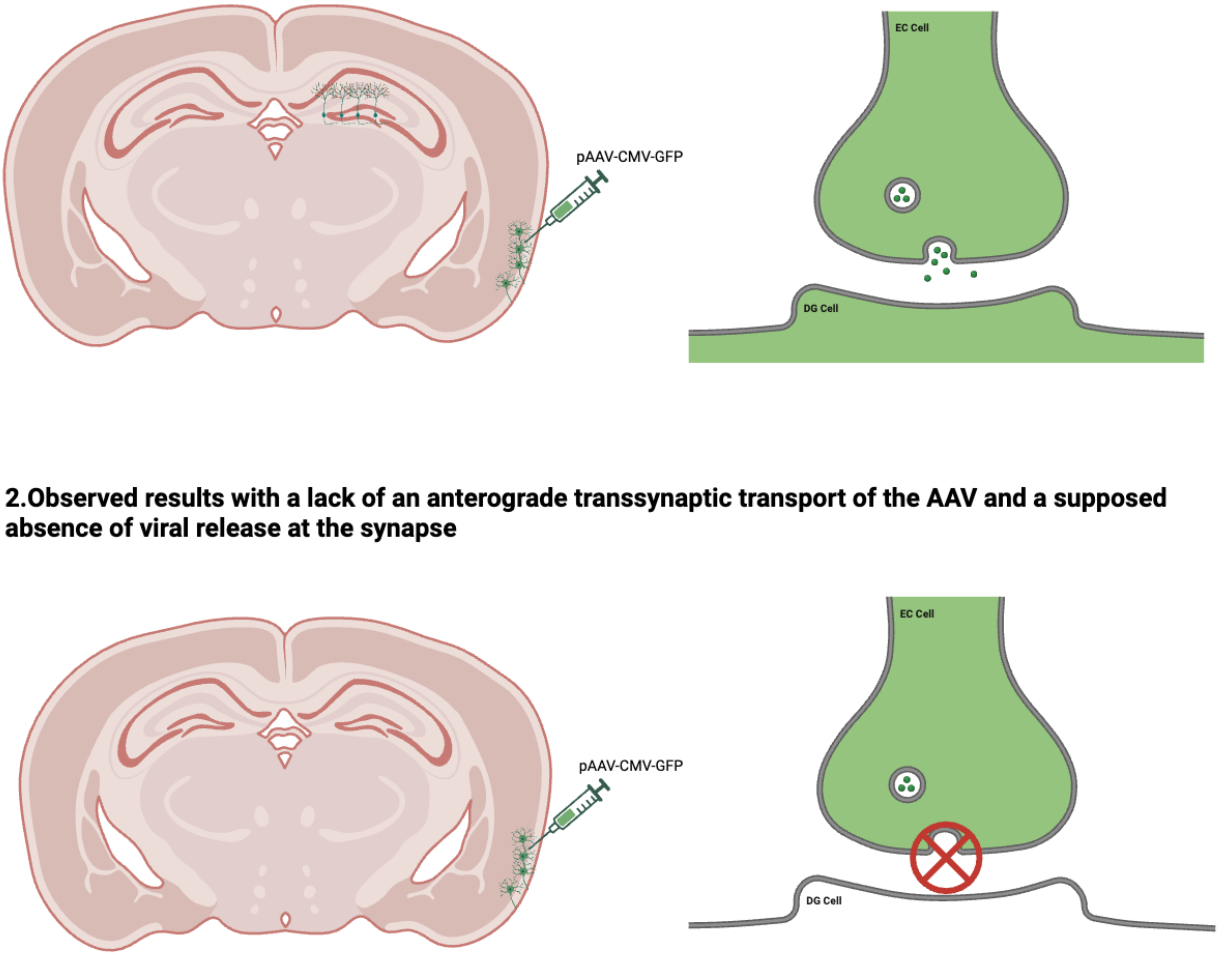


Figure 4-3: Anterograde labeling of entorhinal cortex neurons and projections to the dentate

gyrus. A. Shows the injected structure and the anterograde direction of travel of the virus as well as its coronal representation. **B.** First panel shows a fluorescence image of labeled neurons in the EC with the label put in higher magnification to reveal individual labeled neuronal somata and surrounding neural processes. Brightly labeled EC cell bodies are distributed across the injection site (layer II). The second panel shows a fluorescence image of the dentate gyrus (DG) showing dense axonal labeling from EC neurons within the molecular layer with no labeling of any granule cell. **C.** The first panel shows a labeled cell in the EC and at these lower concentrations, we were unable to detect any labeling in the DG as seen in the second panel. (Made with Biorender)

To overcome signal saturation at the injection site and determine whether the absence of the transsynaptic passage was due to high viral loads inducing cellular stress or cytotoxicity, a systematic dilution series was implemented. The results obtained from the retrograde tracer were used to perform a dilution from $1x10^{13}$ vg/mL to $1x10^{12}$ vg/mL. This was undertaken in order to obtain sparse enough labelling to be quantifiable. The number of cells labelled ranged from 3 to 10 neurons per field, and this successfully resolved the injection site crowding. This demonstrated that the presence of too much label in the molecular layer was not the cause of the lack of synapse jump, since no cells labelled in the DG were detected. (Figure 4.4).



<u>Figure 4.4:</u> Schematic representation of anterograde AAV injection into the EC and the proposed site of transport failure. 1) Left panel shows a coronal section of the mouse brain showing the injection of pAAV-CMV-GFP into the EC and labeled GCs while the right panel shows a schematic of a single EC-DG perforant path synapse illustrating a successful synapse jump with label both in the EC and DG represented the expected outcome of the injection. 2) Left panel shows a coronal slice with the same viral injection but a lack of label in the DG and the right panel shows the point of failure suggested by our results with viral particles successfully filling the EC Cell and following anterograde transport along the axon, but are either not released by the EC cell or captured by the GC across the synaptic cleft, as indicated by the red inhibition symbol. (Made with BioRender)

The subsequent inquiry pertained to the temporal relationship between the injection and the sacrifice of the animal, and whether the brevity of this interval might have precipitated an absence of synaptic jump. In order to conduct a test of this hypothesis, an extension of the waiting period was implemented from two weeks to a month. However, this did not result in the appearance of any labelled granule cells. This finding indicates that additional time does not promote transsynaptic passage in this particular pathway. Immunofluorescence analysis did not yield any positive labelling in the DG, thereby confirming the absence of post-synaptic labelling and indicating that the expression was below the threshold level.

Stepping back from procedural troubleshooting, these results force a deeper interrogation of circuit-specific constraints in viral tracing. We thus seeked to explore the underlying reasons for the termination of AAV1 at the perforant path synapse, given its extensive citation in literature pertaining to its efficient anterograde transsynaptic transfer within subcortical pathways. This technical malfunction gives rise to a number of conceptual questions that are to be examined in future analyses. The impact of the unique composition, or dense matrix, of the perforant path on viral particle release or endocytic capture remains to be elucidated. The question arises as to whether we are observing a more pronounced boundary of AAV-based anterograde transport, wherein specific brain pathways are rendered inaccessible to this specific viral serotype. These questions reframe the data as not just a failed optimisation, but as a critical boundary condition defining the structural selectivity of viral tools in laminar brain regions. This in turn led to the decision to use an alternative viral tracer to verify the results observed with the AAV.

4.2.2. Anterograde labeling of EC using HSV injections

In order to conduct further investigation into circuit connectivity between the EC and the DG, a Herpes Simplex Virus was used. The rationale behind the selection of this HSV lies in its well-researched properties as a transsynaptic tracer, which takes into account its cell tropism, high transgene expression efficiency, and large transgene capacity. Furthermore, in contrast to the bidirectional tendencies of AAVs, HSVs have been documented to travel exclusively in an anterograde direction. Following stereotaxic injections of HSV into layer II of the EC, it was possible to observe a strong labeling of EC layer II neurons. However, as was also the case with our initial observations using the AAV, we noted a total absence of downstream fluorescent labeling within the DG's granule cell layer (see Figure 4-5-B). It is acknowledged that HSV is known to be cytotoxic at a high dose. Therefore, it was hypothesised that this property might be the reason why the virus was not able to travel between synapses. The hypothesis was that the virus would kill the starter cell mechanism before the synaptic jump.

In order to verify whether the high viral concentration and potential local toxicity were the reason for an ineffective transsynaptic passage across the perforant path, a serial dilution series of the viral stock was performed (1:3, 1:9, and 1:27). However, despite the administration of significantly reduced viral titers across these multiple dilutions, no labeled granule cells were observed, even though there was still robust label expression into layer II of the EC and scattered cells in the hilus (see Figure 4-5-C). These findings indicated that the failure of transsynaptic transport is unrelated to viral concentration. Therefore, it can be concluded that it is not a byproduct of localized cytotoxicity at the injection site.

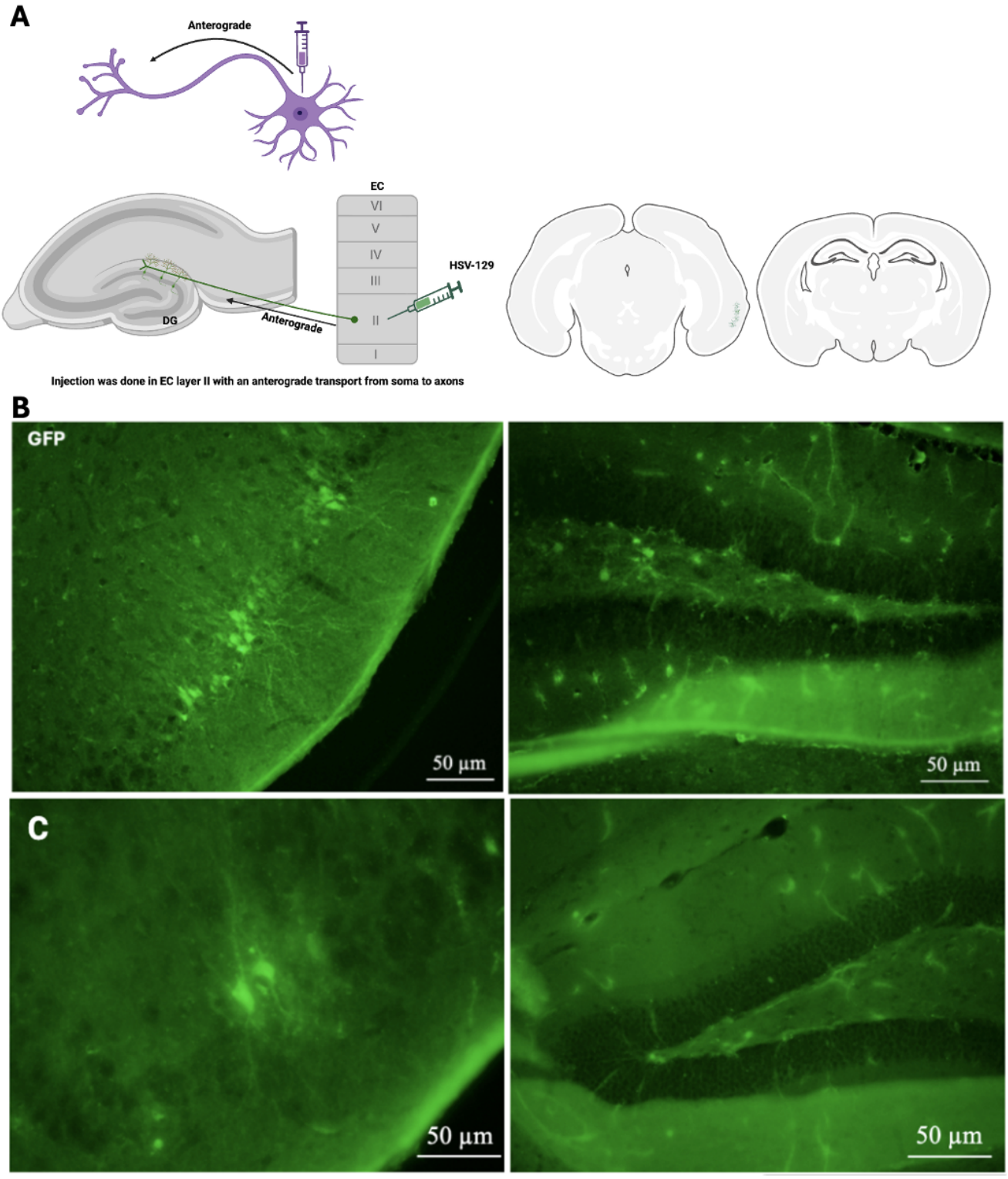


Figure 4-5: Injection of HSV into layer II of the enthorinal cortex. A. Shows the injected structure and the anterograde direction of travel of the virus as well as a coronal representation the mouse EC at the injection sites as well as the mouse hippocampus and the expected outcomes **B.**

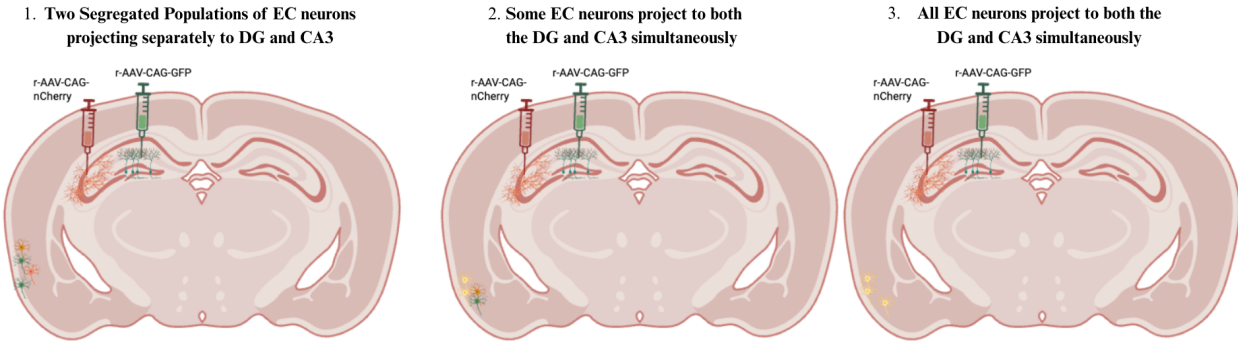
The panel shows well labeled cells in layer II of the EC (confirmed by cresyl violet staining). The second panel shows the dentate gyrus of the same animal, and the absence of any labeled granule cells can be noted even though we can notice the presence of hilar cells. **C.** The first panel shows an injection smaller label of a smaller concentration where we can notice a minimal label of EC cells here showing two cells. The second panel shows just as with the higher concentrations a lack of viral uptake by DG granule cells. (Made with Biorender)

To eliminate the possibility of inaccurate targeting or suboptimal coordinates as the cause of the tracing failure, we performed cresyl violet counterstaining in conjunction with the fluorescence imaging process. This confirmed that our coordinates were successfully targeting layer II of the EC. This finding confirmed that the absence of downstream transsynaptic labeling could not be attributed to mistargeting. This failure pattern was found to be consistent and persistent, with multiple technical adjustments being made, including varied injection coordinates, viral titers, and infusion volumes.

4.3. Double viral injections in DG and CA3

Different studies have previously investigated the perforant path and the structural connections between EC-DG and EC-CA3. It is evident that the direct connection between the EC and the DG is paramount in the "translation" of sensory information received by the hippocampus from the cortex. Furthermore, the role of the EC-CA3 connection in the consolidation of memories and pattern completion is well-established. However, the precise mechanisms through which the EC projects to the CA3 and DG remain to be elucidated. This uncertainty raised the question of whether single EC cells project to the DG and the CA3 at the same time. It is imperative to ascertain the implications of this for the processes of pattern separation and pattern separation. This is due to the fact that it would call into question the necessity of DG in those functions. In the context of

dual projection, three distinct scenarios can be postulated. 1)The existence of two entirely isolated populations of EC layer II neurons evidenced by them projecting separately to the CA3 and the DG. 2) The presence of neurons that demonstrate dual projection, whilst others exhibit a preference for projecting to one of the two structures within the hippocampus. 3) All neurons in the EC project simultaneously to the DG and CA3.



<u>Figure 4-6:</u> Hypothetical models of layer II EC neurons projections to the DG and the CA3. Representation of dual retrograde viral tracing targeted to the DG and CA3. 1. Shows two distinct neuronal populations projecting independently to either the DG (in green) or the CA3 (in orange) showing no overlap. 2. Shows a mixed population with single projecting neurons and dual projecting neurons indicating co-labeled cells (in yellow). 3. Shows a complete collateralization with 100% of cells expressing both fluorescence markers. (Made with Biorender and Canva)

In order to investigate these three possibilities, two retrograde AAVs were used: a GFP-tagged virus injected into the DG and an mCherry-tagged virus injected in the CA3. The employment of this dual-labelling approach facilitated the identification of double-labelled EC neurons, a process achieved by the identification of layer II EC neurons that exhibited the capacity to simultaneously pick up both viruses. Following the administration of AAVs injections to the DG and CA3 regions (see Figure 4-4-B), the results obtained indicated the presence of three distinct neuronal subpopulations. It was possible to identify neurons that only exhibited the

GFP expressed virus, suggesting that they most likely project exclusively to the DG, as indicated by the green labelling. Neurons that only exhibited the mCherry expressed virus were identified, indicating a likelihood of projection exclusively to the CA3 region, as indicated by the orange labelling. Finally, neurons that exhibited the expression of both viruses were observed, suggesting a projection to both the DG and the CA3 regions simultaneously, as indicated by the yellow labelling (Figure 4-4-C). The results indicated that layer II EC neurons do not constitute a homogeneous population exclusively targeting a single, exclusive target rather, they comprise a mixture of functionally segregated circuits, in addition to a collateralised subpopulation. The presence of yellow, double-labelled neurons has been shown to indicate that individual entorhinal neurons simultaneously disseminate information to both the DG and the CA3 region via branched axonal collaterals. This provides an anatomical basis for the simultaneous coordination of the direct perforant path projections. These results thus excluded the first scenario of two distinct segregated populations but still left the possibility of having either the three subpopulations as seen after visualization of the EC or all EC neurons projecting to both hippocampal structures at the same time. The technique employed did not allow for unequivocal confirmation of the validity of either scenario.

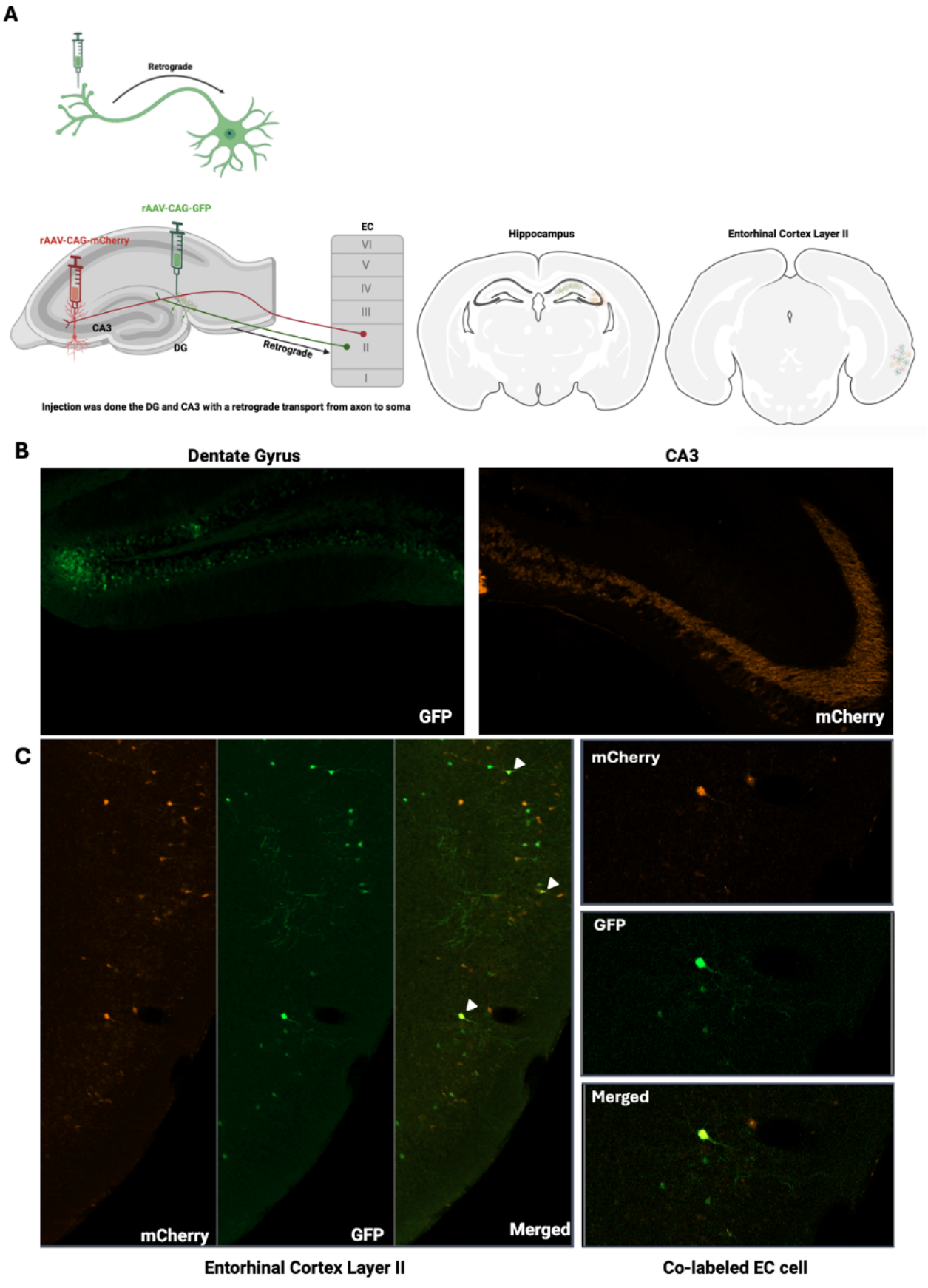

A
Retrograde
rAAV-CAG-GFP
rAAV-CAG-mCherry
EC
VI
V
IV
III
II
I
CA3
DG
Retrograde
Injection was done the DG and CA3 with a retrograde transport from axon to soma
Hippocampus
Entorhinal Cortex Layer II
B
Dentate Gyrus
CA3
GFP
mCherry
C
mCherry
GFP
Merged
mCherry
GFP
Merged
Entorhinal Cortex Layer II
Co-labeled EC cell

Figure 4-7: Retrograde viral circuit mapping of the Entorhinal-Hippocampal Collateralize pathways. A. Shows the injected structures of the DG and CA3 and the direction of travel of the virus as well as its coronal representation at the injection sites as well as the mouse EC and the expected outcomes. **B.** Shows the coronal section of the mouse hippocampus verifying the targeted injection sites with the left panel showing the localized GFP expression to the DG and the right panel showing the mCherry expression in the CA3. **C.** Shows the retrograde labeling of upstream projection neurons in the EC. The first panel show the view of the 488-channel representing only the populations of the neurons projecting to the DG. The second panel shows the view of the 546-channel representing only the population of neurons projecting to the CA3 and the third panel shows the merge of the two channels thus showing the neurons projecting to both subfields in the for of yellow neurons indicated with white arrow heads. **D.** Shows a higher magnification of a dual-labeled collateralized EC neuron.

Given the three distinct neuronal populations obtained through viral double labelling, it was imperative to employ an alternative method to validate the outcomes. In order to accomplish this, a dual injection of dextran Alexa 488 was performed in the DG, in conjunction with a separate injection of dextran miniruby in the CA3. Following the injection of the tracers into both locations, the results were visualised in the EC. This facilitated independent validation of the observations made with the viruses, as the results indicated the presence of the same three subpopulations as previously observed with neurons projecting to the DG, which exclusively absorbed Alexa 488; neurons projecting to the CA3, which exclusively absorbed the miniruby; and neurons projecting to both, which absorbed both dyes (Figure 4-5). This finding serves to substantiate the hypothesis that a subset of neurons within the entorhinal cortex (neurons that exhibited uptake of both tracers) project to both the CA3 and the DG concurrently, while a separate subset of neurons may be projecting to solely one of these structures at any given moment. These results thus provide a framework for further exploration of the structural and functional contributions of the EC and hippocampus in phenomena such as pattern separation and completion.

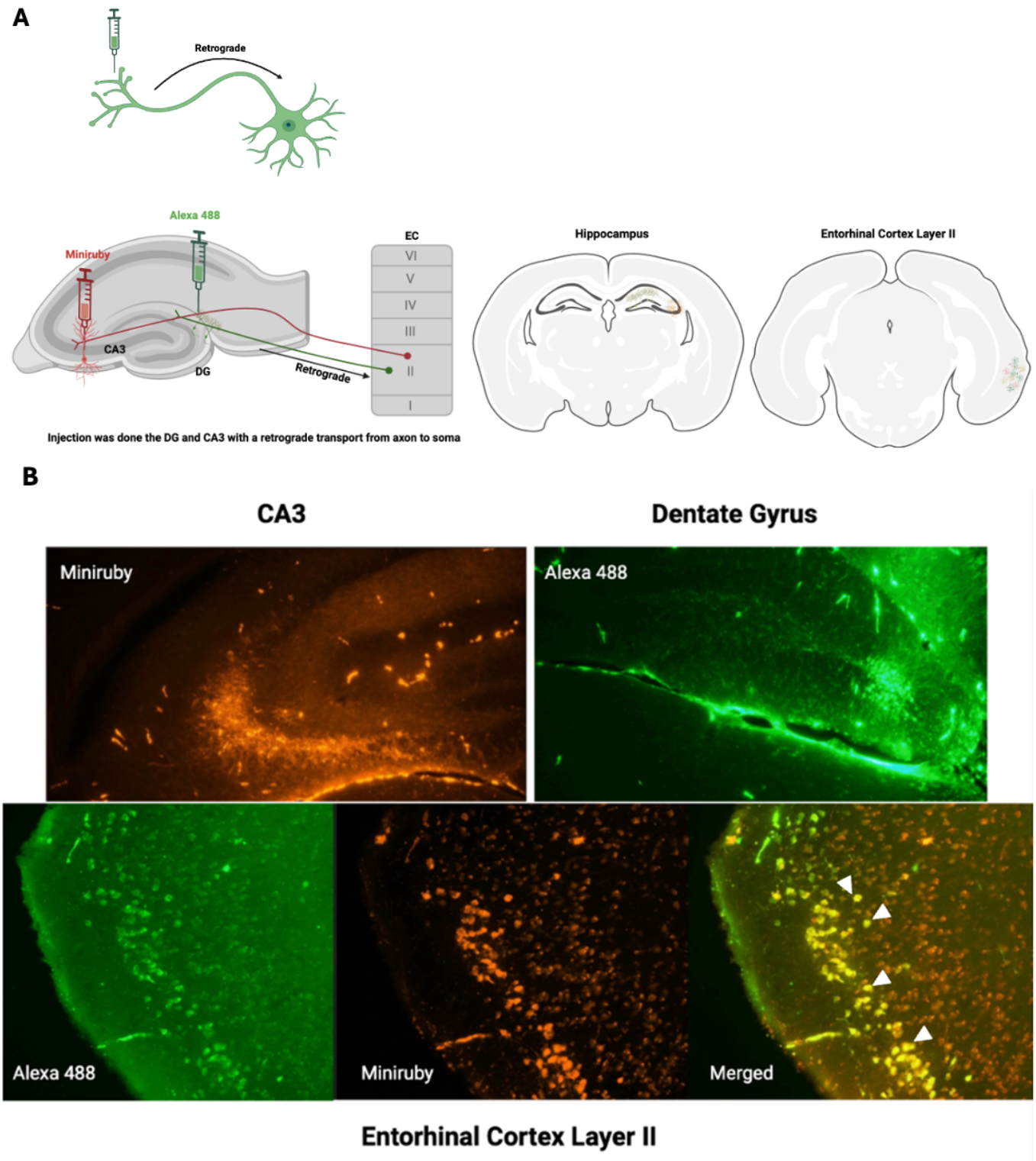


Figure 4-8: Retrograde dextran collateralization between the EC-DG and EC-CA3. The figure shows the coronal section of the mouse hippocampus verifying the targeted injection sites with the left panel showing the localized miniruby expression to the CA3 and the right panel

showing the Alexa 488 expression in the DG. The bottom panels show the retrograde labeling of upstream projection neurons in the EC. The first panel show the view of the miniruby channel representing only the populations of the neurons projecting to the CA3. The second panel shows the view of the Alexa 488 channel representing only the population of neurons projecting to the CA3 and the third panel shows the merge of the two channels thus showing the neurons projecting to both subfields in the form of yellow neurons indicated with white arrow heads.

While the injections successfully demonstrated the existence of dual-projecting neurons, it is imperative to consider the inherent limitations of quantitative analysis. It is evident that retrograde transport efficiency is never absolute; consequently, the absolute number of co-localised cells is likely to underrepresent the true dual-projecting population. This is due to factors such as minute variations in injection volume, slight mismatches in the precise boundaries of the target zones, or differential uptake rates between the AAVs and dextrans used. As previously stated, a cell may project to both the DG and CA3 without being yellow, provided it is not stimulated in both locations. Moreover, even in the event of perfect colocalization, there is a possibility that other unhit neurons may still project individually to the DG and CA3.

5. Discussion

5.1. EC-DG connectivity

The objective of this thesis was to provide answers to two distinct questions regarding the entorhinal-hippocampal circuit. The first objective was to ascertain whether existing tracing tools could be employed to establish a semi-quantitative estimate of the number of connections between EC and the DG. It was demonstrated by the results that the most common forms of viral tracing, both standard retrograde and anterograde, cannot be used to produce an unbiased semi-quantitative estimate of EC-DG connectivity.

The titration experiments conducted with the retrograde AAV injected into the DG demonstrated a dependent relationship between viral concentration and the density of labelled granule cells. An operational window was identified, spanning from 7×10^{9} to 7×10^{10} vg/mL, which resulted in sparse labelling. This finding validated the AAV's behaviour as a concentration-dependent tracer in the DG, aligning with its established usage for sparse retrograde labelling in other regions of the brain (Tervo et al., 2016). However, it should be noted that the interpretation of the EC-DG ratio was not possible on the basis of the sparse labeling in the DG alone. In all of the concentrations and volumes that were examined, the presence of labelled cells in the EC was still observed. It can be posited that the presence of the virus in close proximity to the molecular layer of the dentate gyrus (DG) may be indicative of direct uptake by EC axons, given the anatomical context of layer II EC axons traversing this layer en route to their targets. It can be hypothesised that the direct uptake would likely be reflected in the same way if a transynaptic virus were to be used, since some of the labelled EC cells would be a result of direct uptake rather than true retrograde transport from a synapse formed on a labelled granule cell. The findings of this study indicate that the discrepancy highlighted by Amaral et al. (1990) concerning the absence of direct anatomical evidence for the number of synapses formed by a single entorhinal neuron onto the dentate gyrus, has persisted.

This is not due to a lack of interest, but rather due to the fact that the most readily available tools for tracing are not appropriate for resolving this issue in a region where the afferent fibres of interest travel directly through the target zone. The reduction of volume and concentration has been shown to exert control over the number of postsynaptically labeled granule cells; however, it has been demonstrated that this process is not capable of discriminating between a synaptic connection and a fiber of passage in isolation. Consequently, any ratio calculated by dividing labelled EC neurons by labelled DG neurons under these conditions would systematically overestimate our quantification. The degree of overestimation would be impossible to correct for without an independent method of confirming synaptic contact, such as paired recordings, electron microscopy, etc.

Upon determining that the retrograde tracing from the DG had been compromised by axons of passage, the anterograde route appeared to be the more appropriate one for addressing the same question by inverting it. In the case of anterograde transport, the virus would be taken up by the EC soma and released at its own terminals which would eliminate the confounding variable. However, the results obtained from the two anterograde viruses employed in this study did not correspond with the anticipated outcomes. The injection of an AAV1 into layer II of the EC resulted in the observation of dense axonal labeling throughout the molecular layer of the DG, thereby confirming that the injected neurons project to the anticipated target. Nonetheless, notwithstanding the execution of a series of titration trials and the implementation of an augmented wait period between the surgical intervention and perfusion, no instance of granule cell labelling was observed. This outcome was replicated with HSV, despite its selection due to its proposed unidirectionality. This failure of two distinct viral tools is informative in its own right since AAV1's capacity for anterograde transsynaptic spread and HSV's capacity for fast anterograde transport have both been

demonstrated in other circuits (Jones et al., 1997; Smith et al., 2000). A salient issue that is brought to light by these data is the restricted operational window for both the HSV and the AAV1 in this particular pathway. The employment of AAV1 necessitates the injection of high titers, as these are required to trigger transsynaptic transfer. A loss of transsynaptic properties is observed when the genomic copy concentration falls below a strict threshold (Zingg et al., 2020), a phenomenon that engenders a technical paradox in the present experiment. At full concentrations, both viruses induced a dense accumulation of overlapping cells in the DG's molecular layer. However, the signal did not cross to the GC layer. While elevated viral titers have been demonstrated to induce local toxicity, which can impede the cell's intracellular machinery required for axonal transport and vesicular release (Zingg et al., 2022), our systematic dilutions (1:3 to 1:27) have effectively ruled out this possibility. This finding indicates that the observed failures are not attributable to the viruses but rather give rise to a number of conceptual questions that are to be examined in future analyses. The synapses formed by EC cells onto granule cells in the molecular layer exhibit significant structural and molecular distinctions from numerous circuits in which AAV1 and HSV transsynaptic spread have been previously validated. AAV1 is a well-known anterograde tracer that has been extensively studied in various brain regions. However, recent research has revealed that its transduction efficiency is circuit-dependent and contingent on the molecular composition of the target synapse (Zingg et al., 2020). It might be conceivable that the specific endocytic or membrane trafficking machinery on which these viruses depend for transsynaptic transfer is not accessible in the same way at the perforant path synapse. This hypothesis is plausible because of the failure of at least two viral families that were tested to label granule cells. Such assumptions would need to be tested in other pathways under the same conditions as the ones used during or experiments to determine the rationality of that hypothesis.

When considered collectively, the retrograde and anterograde results reach the same conclusion: that conventional AAVs and pseudo-rabies-family viruses are inadequate for the purpose of generating a quantitative estimate of EC-DG connectivity. On the retrograde side, the issue lies in the specificity of the problem, where there is sparse labelling, but no distinction can be made between synaptic spread and axonal passage. On the anterograde side, the missing step seems to be the jump at the perforant path synapse itself. It is imperative to interpret these setbacks not as unsuccessful pilot experiments, but rather as informative negative results that offer valuable insights for future improvements. This has a direct methodological consequence for any future attempts to quantify this circuit. The quantification of these connections is likely to require either a starter cell-restricted, complementation-dependent monosynaptic system, such as glycoprotein-deleted rabies virus paired with a helper virus to create a single synapse jump, or a non-viral strategy that is not subject to the biological gating step that appears to block AAVs and HSVs at this synapse. An alternative non-viral strategy could be intracellular filling of a single identified granule cell followed by electron microscopy to directly count entorhinal boutons on a reconstructed dendritic tree.

5.2. EC collateralization

The second objective of this thesis was to determine whether individual layer II EC neurons send collateral projections to both the DG and CA3. A thorough review of the pertinent literature revealed that these questions had not been addressed in a systematic manner. Moreover, this question is complementary to the previous one insofar as any quantitative model in the perforant path is rendered more meaningful if we are also able to understand whether the neurons contributing to this model focus only on a single downstream target or if they would distribute the same cortical signal across the hippocampal formation. While employing dual labelling with a

retrograde AAV-GFP in the DG and retrograde AAV-mCherry in the CA3, three subpopulations of layer II EC neurons were consistently observed: those with cells labelled with GFP only, those with cells labelled with mCherry only, and a smaller population of double-labelled yellow cells. This finding indicated the presence of a distinct subpopulation of EC layer II neurons that exhibited dual projection, alongside two other subpopulations of neurons that demonstrated selective infection by one of the viruses. These results thus argue against two strictly segregated streams of the EC's projection to the DG and the CA3. The presence of this third population was reproduced independently using fluorescent conjugated dextrans, whose transport does not depend on receptor tropism, promoter activity, or viral packaging. Using an alternative tracer that is not subject to the same biases that could affect the viral serotypes helped us confirm the results we had with the viral tracers. The consistency between the results from the viral and dextran injections on the three populations in question, provide substantial evidence that the double-labelled cells are the result of a real collateralisation rather than an artefact specific to either the virus or the dextran.

Previous anatomical work showed that the EC projections to the DG and CA3 both come mostly from layer II but never resolved whether they arise from the same neuronal pool or different cells (Witter et al., 1989; Tamamaki and Nojyo, 1993). Our results thus directly address the missing information of those previous studies. As mentioned before, our findings rule out the simplest of the three models we set out to distinguish, namely the hypothesis of two entirely segregated neuronal pools with no overlap. However, they do not, allow us to differentiate between the remaining two possibilities of either a real mixed population containing both single and dual-projecting neurons as the data suggests or a case where all layer II EC neurons collateralise to both the DG and the CA3 simultaneously. To determine which scenario is accurate, it could be interesting to employ a method that reports the possible collateralisation of an individual cell or a

couple of cells at a time. For example, by using single-cell reconstruction of a randomly sampled population of layer II neurons, as opposed to a dual bulk injection strategy, we would be able to follow each neuron individually and report any presence or absence of collateralisation. The tracking of a single cell would be particularly interesting, as it would help circumvent the limitations of the retrograde transport process, whether if it is viral or involving dextrans. Those limitations are due to the fact that minor variations in injection volume, imprecise alignment of injections to the DG and CA3, or even different uptake efficiency between the two AAVs or the two dextrans, could cause that a neuron that genuinely projects to both structures could easily be captured by only one tracer thus classifying it inaccurately as a single projecting neuron. Therefore, it is imperative to interpret the proportions of the three subpopulations reported here as a qualitative demonstration of collateralisation rather than a quantitative estimate of the proportion of layer II EC neurons that collateralise.

Either interpretation of scenario 2 that some but not all layer II EC neurons collateralise or scenario 3 that all EC layer II collateralise to both structures, have implications for how the DG and CA3 could be viewed in regard to their functions. As a matter of fact, they are usually treated as functionally distinct stations in the trisynaptic loop, one specialized for pattern separation and the other for pattern completion (Marr, 1971; Yassa and Stark, 2011). The identification of the three neuronal populations could potentially indicate a semi-segregated network, which could imply the possibility that the DG and CA3 are complementary in their roles. Indeed, since studies lesioning the DG showed impaired spatial separation only (Kesner et al., 2004), it could be speculated that collateralising neurons are responsible for multiple types of separation, thus showing the role of the CA3 not only in pattern completion but also in pattern separation (Rolls, 2013). This prompts the question of the extent to which the CA3 is capable of replicating the functions of the DG which

in turn gives rise to the question of whether the CA3 could serve as a backup and assume certain roles of the DG in the event of its impairment. Those interpretations suggest that some cells in the DG and CA3 have the ability to receive different inputs from segregated streams of layer II EC neurons projections while some cells in both structures receive the same data from the same EC cell. This dual-projection network may be responsible for non-spatial forms of separation, thereby broadening our understanding of the CA3's computational roles.

Furthermore, if a subset of entorhinal neurons broadcasts an identical cortical signal simultaneously into both the indirect, DG mediated trisynaptic pathway and the direct EC-CA3 monosynaptic pathway, it could mean that at least part of the pattern separated code received by the CA3 from the DG and part of the raw, unseparated data that supports pattern completion in CA3 may originate from the same upstream neuron. This brings up the question of if the CA3's ability to reconcile a sparse, separated signal from the DG with a dense, direct cue from the EC could, for a specific set of inputs, involve a comparison of a transformed and an untransformed copy of the same original signal, a hypothesis that would need to be investigated further. Our data provides one of the first pieces of evidence that, some cells in the EC are responsible for the same cue being received by the CA3 and the DG at the same time, rather than two anatomically independent circuits.

Future research could extend the dual-labelling collateralisation experiments towards single-cell resolution. A complementary step towards single-cell resolution is already available in the form of the Janelia MouseLight database, which contains complete axonal reconstructions of individually labelled projection neurons registered to the Allen Common Coordinate Framework (Winnubst et al., 2019). The MouseLight NeuronBrowser currently provides access to reconstructed neurons with somata in the EC. As each of these reconstructions shows the complete axonal arbor of a

single identified cell, they provide a form of evidence that is not subject to the limitations in co-labeling efficiency of our bulk dual-retrograde approach. Consequently, as opposed to determining the collateralization from the proportion of neurons picking up two independently injected tracers, it is possible to directly examine whether a single reconstructed axon has terminal branches within both the molecular layer of the DG and the pyramidal cell layer of CA3. This would provide an independent, tracer-free cross-check of the three-population model proposed here. If a given neuron's arbor includes collaterals to both structures, this would corroborate the existence of dual-projecting neurons at the single-cell level. Moreover, if the sampled neurons instead innervate only one target each, this would not contradict our findings, given the small sample size, but would help in showing how some EC cells also send segregated signals to DG and CA3 (Figure 5). Layer II is predominantly constituted of Reelin-positive stellate cells and Calbindin-positive pyramidal cells (Witter et al., 2017). Consequently, the employment of a single cell morphological reconstruction would facilitate the determination of whether dual projecting layer II EC neurons constitute a molecularly distinct cell type or a random subset of the cell population in the EC. Furthermore, this approach would enable the assessment of whether the proportion of collateralization would differ between MEC and LEC. Advancement in this area would facilitate the evolution of the field towards a quantitative structural baseline which is a fundamental objective of this thesis.

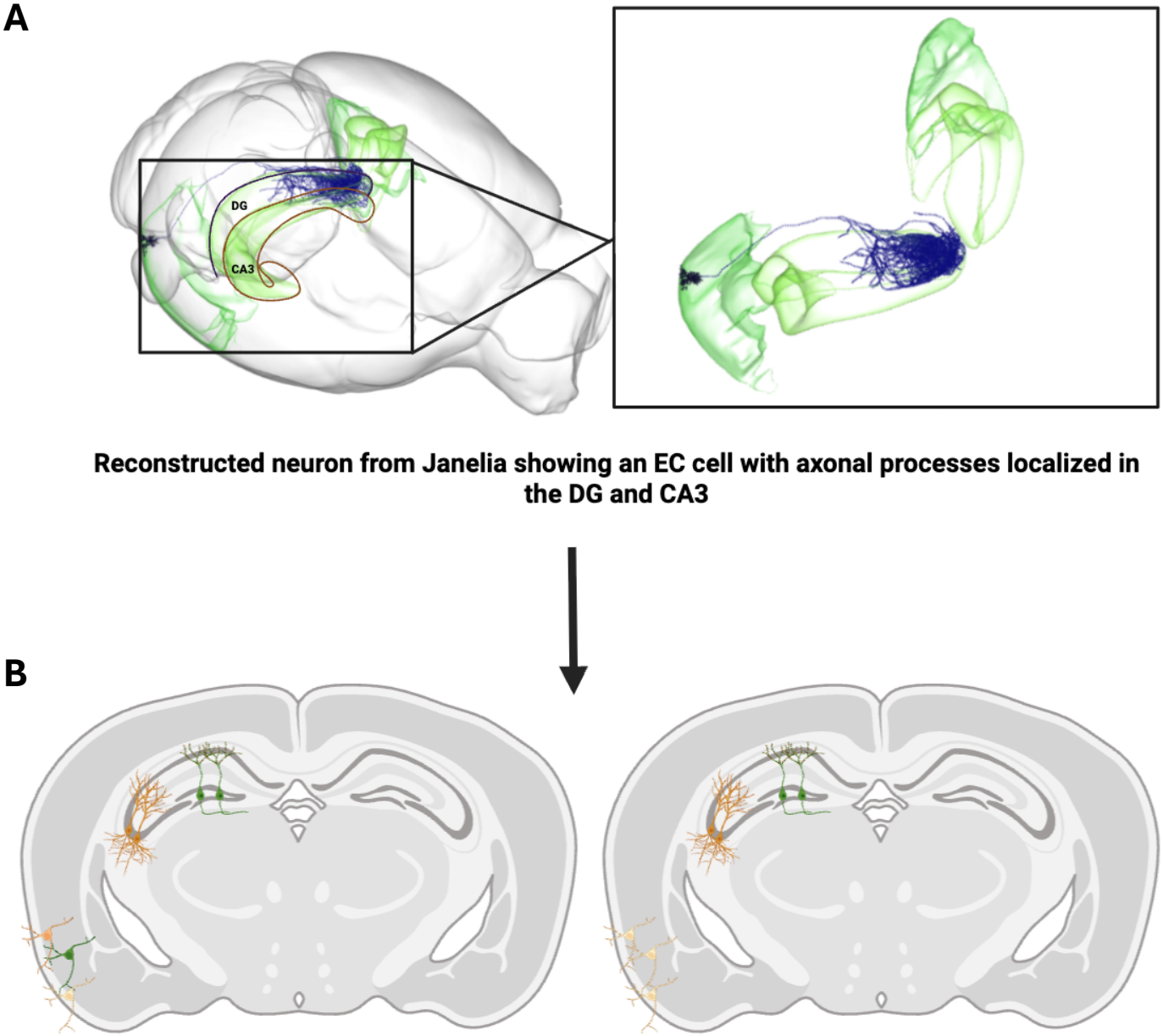


Figure 5: Structural corroboration of EC projections to the DG and CA3. A. Shows a 3D reconstruction of a EC neuron from Janelia NeuronLight database with an axonal arborizations to the DG and CA3 thus leading to the corroboration of B. Showing two of the possible scenarios we determined possible for layer II EC neurons dual projections to the DG and CA3.

6. Conclusion

The EC and the hippocampus are among the most extensively studied circuits in the mammalian brain. However, the precise structural connections that dictate how information is transmitted from the EC to the DG and how that same cortical input is distributed across the trisynaptic and monosynaptic pathways of the hippocampus have remained mostly qualitative. The objective of this thesis was to address this gap by establishing the following objectives: firstly, to determine which tracing strategies can provide a semi-quantitative estimate of entorhinal-dentate connectivity; and secondly, to test directly whether individual layer II entorhinal neurons collateralise to both the DG and the CA3. This thesis demonstrated that the tools most readily available for transsynaptic tracing are not adequate in their standard form. Injecting a retrograde AAV into the DG demonstrated the possibility of diluting the virus to sparsely label individual granule cells. However, it was not possible to discriminate between a genuine synaptic jump between the DG and EC versus a label where an axon merely passes through the injection site, given that perforant path fibres travel directly through the molecular layer of the DG. The injection of anterograde AAV1 and HSV into layer II of the EC resulted in the labelling of EC cells and their axon terminals within the molecular layer. However, despite varying the concentration, volume, and incubation time of the viruses, no labelled granule cell was produced. The observation that this outcome was consistent across two mechanistically distinct viral families suggested that the phenomenon may be indicative of a specific property to transsynaptic spread at the perforant path synapse, rather than a simple failure of optimization. This supposition would then need to be explored in future analysis that would compare the efficiency of the virus to jump other synaptic pathways under the same condition. When considered as a whole, these results reframe the original question and establish in a systematic way which classes of tracer are not suited to this circuit and why. Furthermore, it identifies the properties a future virus will need, such as a mechanism that

depends on an actual synaptic event rather than just axonal proximity. With regard to the second objective, the results obtained were more directly conclusive. The employment of two distinct retrograde tracing methodologies resulted in the identification of a population of double-labeled layer II entorhinal neurons, in addition to separate populations that were labeled from a single one of the two injected structures. The results indicated that EC projections to the DG and CA3 do not originate from two entirely distinct neuronal pools. Furthermore, it was demonstrated that at least a subset of EC neurons transmits the same upstream cortical signal into both regions, which are responsible for pattern separation and pattern completion. This is, to the best of our knowledge, one of the first documented instances of such collateralisation in this circuit, and it carries a direct implication for how these two regions are thought to be coordinated. Collectively, these two objectives form the basis for future quantification studies, thereby establishing that the entorhinal cortex's output to the hippocampus is anatomically heterogeneous rather than cleanly compartmentalised by target. Future research should build on the quantification of connectivity and the collateralization evidence presented here, moving towards single cell resolution methods capable of both confirming synaptic contact directly and establishing what proportion of the entorhinal population is actually dual projecting. This would bring researchers closer to a genuinely quantitative structural account of how the entorhinal cortex organizes information spread across the hippocampal formation.

7. References

Amaral DG, Ishizuka N, Claiborne B. Neurons, numbers and the hippocampal network. Prog Brain Res. 1990;83:1-11. doi: 10.1016/s0079-6123(08)61237-6. PMID: 2203093.

Amaral DG, Schumann CM, Nordahl CW. Neuroanatomy of autism. Trends Neurosci. 2008 Mar;31(3):137-45. doi: 10.1016/j.tins.2007.12.005. Epub 2008 Feb 6. PMID: 18258309.

Amaral DG, Witter MP. The three-dimensional organization of the hippocampal formation: a review of anatomical data. Neuroscience. 1989;31(3):571-91. doi: 10.1016/0306-4522(89)90424-7. PMID: 2687721.

Andersen P, Bliss TV, Skrede KK. Lamellar organization of hippocampal pathways. Exp Brain Res. 1971;13(2):222-38. doi: 10.1007/BF00234087. PMID: 5570425.

Arellano JI, Rakic P. Updated Neuronal Numbers of the Rat Hippocampal Formation: Redesigning the Hippocampal Model. Hippocampus. 2026 Jan;36(1):e70070. doi: 10.1002/hipo.70070. PMID: 41549060; PMCID: PMC12812505.

Bakker A, Kirwan CB, Miller M, Stark CE. Pattern separation in the human hippocampal CA3 and dentate gyrus. Science. 2008 Mar 21;319(5870):1640-2. doi: 10.1126/science.1152882. PMID: 18356518; PMCID: PMC2829853.

Basu J, Siegelbaum SA. The Corticohippocampal Circuit, Synaptic Plasticity, and Memory. Cold Spring Harb Perspect Biol. 2015 Nov 2;7(11):a021733. doi: 10.1101/cshperspect.a021733. PMID: 26525152; PMCID: PMC4632668.

BLACKSTAD TW. Commissural connections of the hippocampal region in the rat, with special reference to their mode of termination. J Comp Neurol. 1956 Oct;105(3):417-537. doi: 10.1002/cne.901050305. PMID: 13385382.

Bonfanti L, Peretto P. Adult neurogenesis in mammals--a theme with many variations. Eur J Neurosci. 2011 Sep;34(6):930-50. doi: 10.1111/j.1460-9568.2011.07832.x. PMID: 21929626.

Bromer C, Bartol TM, Bowden JB, Hubbard DD, Hanka DC, Gonzalez PV, Kuwajima M, Mendenhall JM, Parker PH, Abraham WC, Sejnowski TJ, Harris KM. Long-term potentiation expands information content of hippocampal dentate gyrus synapses. Proc Natl Acad Sci U S A. 2018 Mar 6;115(10):E2410-E2418. doi: 10.1073/pnas.1716189115. Epub 2018 Feb 20. PMID: 29463730; PMCID: PMC5877922.

Cajal, S. R. (1888). Estructura de los centros nerviosos de las aves. Rev. Trim. Histol. Norm. Patol. 1, 1–10.

Canto CB, Wouterlood FG, Witter MP. What does the anatomical organization of the entorhinal cortex tell us? Neural Plast. 2008;2008:381243. doi: 10.1155/2008/381243. PMID: 18769556; PMCID: PMC2526269.

Card JP, Enquist LW (2014) Transneuronal circuit analysis with pseudorabies viruses. Curr Protoc Neurosci 68:1.5.1–1.5.39. pmid:24984685

Cherubini E, Miles R. The CA3 region of the hippocampus: how is it? What is it for? How does it do it? Front Cell Neurosci. 2015 Feb 5;9:19. doi: 10.3389/fncel.2015.00019. PMID: 25698930; PMCID: PMC4318343.

Cholvin, T., Bartos, M. The dentate gyrus efficiently converges LEC and MEC inputs into multimodal, highly specific and reliable environmental representations. Nat Neurosci 29, 1166–1180 (2026). https://doi.org/10.1038/s41593-026-02240-0

Cucchiaro JB, Uhlrich DJ. Phaseolus vulgaris leucoagglutinin (PHA-L): a neuroanatomical tracer for electron microscopic analysis of synaptic circuitry in the cat's dorsal lateral geniculate nucleus. J Electron Microsc Tech. 1990 Aug;15(4):352-68. doi: 10.1002/jemt.1060150405. PMID: 2391562.

Deepl translate and Deepl write. 2026 https://www.deepl.com/en/write

Ericson H, Blomqvist A. (1988) Tracing of neuronal connections with cholera toxin subunit B: light and electron microscopic immunohistochemistry using monoclonal antibodies. J Neurosci Methods. 1988 Jul;24(3):225-35. doi: 10.1016/0165-0270(88)90167-7. PMID: 2458510.

Fink RP, Heimer L. Two methods for selective silver impregnation of degenerating axons and their synaptic endings in the central nervous system. Brain Res. 1967 Apr;4(4):369-74. doi: 10.1016/0006-8993(67)90166-7. PMID: 4166480.

García-López P, García-Marín V, Freire M. The discovery of dendritic spines by Cajal in 1888 and its relevance in the present neuroscience. Prog Neurobiol. 2007 Oct;83(2):110-30. doi: 10.1016/j.pneurobio.2007.06.002. Epub 2007 Jun 19. PMID: 17681416.

Germroth P, Schwerdtfeger WK, Buhl EH. GABAergic neurons in the entorhinal cortex project to the hippocampus, Brain Research, Volume 494, Issue 1, 1989, Pages 187-192, ISSN 0006-8993, https://doi.org/10.1016/0006-8993(89)90162-5.

Gilbert PE, Kesner RP, Lee I. Dissociating hippocampal subregions: double dissociation between dentate gyrus and CA1. Hippocampus. 2001;11(6):626-36. doi: 10.1002/hipo.1077. PMID: 11811656.

Gold AE, Kesner RP. (2005). The role of the CA3 subregion of the dorsal hippocampus in spatial pattern completion in the rat. Hippocampus 15 808–814

Goodrich-Hunsaker NJ, Hunsaker MR, Kesner RP. The interactions and dissociations of the dorsal hippocampus subregions: how the dentate gyrus, CA3, and CA1 process spatial information. Behav Neurosci. 2008 Feb;122(1):16-26. doi: 10.1037/0735-7044.122.1.16. PMID: 18298245.

Hagihara H, Toyama K, Yamasaki N, Miyakawa T. Dissection of hippocampal dentate gyrus from adult mouse. J Vis Exp. 2009 Nov 17;(33):1543. doi: 10.3791/1543. PMID: 19920804; PMCID: PMC3142893.

Henze D, Wittner L, Buzsáki G. Single granule cells reliably discharge targets in the hippocampal CA3 network in vivo. Nat Neurosci 5, 790–795 (2002). https://doi.org/10.1038/nn887

Hui Y, Zheng X, Zhang H, et al. Strategies for Targeting Neural Circuits: How to Manipulate Neurons Using Virus Vehicles. Frontiers in Neural Circuits. 2022 ;16:882366. DOI: 10.3389/fncir.2022.882366. PMID: 35571271; PMCID: PMC9099413.

Jinde S, Zsiros V, Jiang Z, Nakao K, Pickel J, Kohno K, Belforte JE, Nakazawa K. Hilar mossy cell degeneration causes transient dentate granule cell hyperexcitability and impaired pattern separation. Neuron. 2012 Dec 20;76(6):1189-200. doi: 10.1016/j.neuron.2012.10.036. PMID: 23259953; PMCID: PMC3530172.

Kawamura T, Nair RR, Tsutsui KI, Ohara S. Mapping mouse hippocampal output circuits using direction-selective anterograde transsynaptic transduction. doi: https://doi.org/10.64898/2026.05.13.724828

Kerr KM, Agster KL, Furtak SC, Burwell RD. Functional neuroanatomy of the parahippocampal region: the lateral and medial entorhinal areas. Hippocampus. 2007;17(9):697-708. doi: 10.1002/hipo.20315. PMID: 17607757.

Kesner RP. A process analysis of the CA3 subregion of the hippocampus. Front Cell Neurosci. 2013 May 27;7:78. doi: 10.3389/fncel.2013.00078. PMID: 23750126; PMCID: PMC3664330.

Kesner RP, Lee I, Gilbert P. A behavioral assessment of hippocampal function based on a subregional analysis. Rev Neurosci. 2004;15(5):333-51. doi: 10.1515/revneuro.2004.15.5.333. PMID: 15575490.

Knierim JJ, Neunuebel JP, Deshmukh SS. Functional correlates of the lateral and medial entorhinal cortex: objects, path integration and local-global reference frames. Philos Trans R Soc Lond B Biol Sci. 2013 Dec 23;369(1635):20130369. doi: 10.1098/rstb.2013.0369. PMID: 24366146; PMCID: PMC3866456.

Kunec S, Hasselmo ME, Kopell N. Encoding and Retrieval in the CA3 Region of the Hippocampus: A Model of Theta-Phase Separation. Journal of Neurophysiology 2005 94:1, 70-82 10.1152/jn.00731.2004

Lavenex P, Amaral DG. Hippocampal-neocortical interaction: a hierarchy of associativity. Hippocampus. 2000;10(4):420-30. doi: 10.1002/1098-1063(2000)10:4<420::AID-HIPO8>3.0.CO;2-5. PMID: 10985281.

Lazarov O, Hollands C. Hippocampal neurogenesis: Learning to remember, Progress in Neurobiology, Volumes 138–140, 2016, Pages 1-18, ISSN 0301-0082, https://doi.org/10.1016/j.pneurobio.2015.12.006.

Leutgeb JK, Leutgeb S, Moser MB, Moser EI. Pattern separation in the dentate gyrus and CA3 of the hippocampus. Science. 2007 Feb 16;315(5814):961-6. doi: 10.1126/science.1135801. PMID: 17303747.

Lopez-Rojas J, Kreutz MR. Mature granule cells of the dentate gyrus--Passive bystanders or principal performers in hippocampal function? Neurosci Biobehav Rev. 2016 May;64:167-74. doi: 10.1016/j.neubiorev.2016.02.021. Epub 2016 Mar 3. PMID: 26949226.

Lorente de Nò, R. (1934) Studies on the Structure of the Cerebral Cortex II. Continuation of the Study of the Ammonic System. Journal für Psychologie und Neurologie, 46, 113-177.

Maass A, Düzel S, Goerke M, Becke A, Sobieray U, Neumann K, Lövden M, Lindenberger U, Bäckman L, Braun-Dullaeus R, Ahrens D, Heinze HJ, Müller NG, Düzel E. Vascular hippocampal plasticity after aerobic exercise in older adults. Mol Psychiatry. 2015 May;20(5):585-93. doi: 10.1038/mp.2014.114. Epub 2014 Oct 14. PMID: 25311366.

Marr D. Simple memory: a theory for archicortex. Philos Trans R Soc Lond B Biol Sci. 1971 Jul 1;262(841):23-81. doi: 10.1098/rstb.1971.0078. PMID: 4399412.

McHugh TJ, Jones MW, Quinn JJ, Balthasar N, Coppari R, Elmquist JK, Lowell BB, Fanselow MS, Wilson MA, Tonegawa S. Dentate gyrus NMDA receptors mediate rapid pattern separation in the hippocampal network. Science. 2007 Jul 6;317(5834):94-9. doi: 10.1126/science.1140263. Epub 2007 Jun 7. PMID: 17556551.

McNaughton BL, Barnes CA, Andersen P. Synaptic efficacy and EPSP summation in granule cells of rat fascia dentata studied in vitro. Journal of Neurophysiology 1981 46:5, 952-966 10.1152/jn.1981.46.5.952

Miller JF, Fried I, Suthana N, Jacobs J. Repeating spatial activations in human entorhinal cortex. Curr Biol. 2015 Apr 20;25(8):1080-5. doi: 10.1016/j.cub.2015.02.045. Epub 2015 Apr 2. PMID: 25843029; PMCID: PMC4422049.

Nakashiba T, Buhl DL, McHugh TJ, Tonegawa S. Hippocampal CA3 output is crucial for ripple-associated reactivation and consolidation of memory. Neuron. 2009 Jun 25;62(6):781-7. doi: 10.1016/j.neuron.2009.05.013. PMID: 19555647; PMCID: PMC2728553.

Nakashiba T, Cushman JD, Pelkey KA, Renaudineau S, Buhl DL, McHugh TJ, Rodriguez Barrera V, Chittajallu R, Iwamoto KS, McBain CJ, Fanselow MS, Tonegawa S. Young dentate granule cells mediate pattern separation, whereas old granule cells facilitate pattern completion. Cell. 2012 Mar 30;149(1):188-201. doi: 10.1016/j.cell.2012.01.046. Epub 2012 Feb 23. PMID: 22365813; PMCID: PMC3319279.

Nakazawa K, Quirk MC, Chitwood RA, Watanabe M, Yeckel MF, Sun LD, Kato A, Carr CA, Johnston D, Wilson MA, Tonegawa S. Requirement for hippocampal CA3 NMDA receptors in associative memory recall. Science. 2002 Jul 12;297(5579):211-8. doi: 10.1126/science.1071795. Epub 2002 May 30. PMID: 12040087; PMCID: PMC2877140.

NAUTA WJ. Selective silver impregnation of degenerating axons in the central nervous system. Stain Technol. 1952 May;27(3):175-9. doi: 10.3109/10520295209105080. PMID: 14958510.

Navarro Schröder T, Haak KV, Zaragoza Jimenez NI, Beckmann CF, Doeller CF. Functional topography of the human entorhinal cortex. Elife. 2015 Jun 8;4:e06738. doi: 10.7554/eLife.06738. PMID: 26052748; PMCID: PMC4458840.

Neves G, Cooke SF, Bliss TV. Synaptic plasticity, memory and the hippocampus: a neural network approach to causality. Nat Rev Neurosci. 2008 Jan;9(1):65-75. doi: 10.1038/nrn2303. Erratum in: Nat Rev Neurosci. 2012 Dec;13(12):878. PMID: 18094707.

Norman KA. How hippocampus and cortex contribute to recognition memory: revisiting the complementary learning systems model. Hippocampus. 2010 Nov;20(11):1217-27. doi: 10.1002/hipo.20855. PMID: 20857486; PMCID: PMC3416886.

Norman KA, O'Reilly RC. Modeling hippocampal and neocortical contributions to recognition memory: a complementary-learning-systems approach. Psychol Rev. 2003 Oct;110(4):611-46. doi: 10.1037/0033-295X.110.4.611. PMID: 14599236.

Ohara S, Inoue K, Witter MP, Iijima T. Untangling neural networks with dual retrograde transsynaptic viral infection. Front Neurosci. 2009 Dec 15;3(3):344-9. doi: 10.3389/neuro.01.032.2009. PMID: 20198151; PMCID: PMC2796918.

PENFIELD W, MILNER B. Memory deficit produced by bilateral lesions in the hippocampal zone. AMA Arch Neurol Psychiatry. 1958 May;79(5):475-97. doi: 10.1001/archneurpsyc.1958.02340050003001. PMID: 13519951.

Popov VI, Stewart MG. Complexity of contacts between synaptic boutons and dendritic spines in adult rat hippocampus: three-dimensional reconstructions from serial ultrathin sections in vivo. Synapse. 2009 May;63(5):369-77. doi: 10.1002/syn.20613. PMID: 19173264.

Qiu L, Zhang B, Gao Z. Lighting Up Neural Circuits by Viral Tracing. Neurosci Bull. 2022 Nov;38(11):1383-1396. doi: 10.1007/s12264-022-00860-7. Epub 2022 May 16. PMID: 35578093; PMCID: PMC9672192.

Rolls ET. The mechanisms for pattern completion and pattern separation in the hippocampus. Front Syst Neurosci. 2013 Oct 30;7:74. doi: 10.3389/fnsys.2013.00074. PMID: 24198767; PMCID: PMC3812781.

Saleeba C, Dempsey B, Le S, Goodchild A, McMullan S. A Student's Guide to Neural Circuit Tracing. Front Neurosci. 2019 Aug 27;13:897. doi: 10.3389/fnins.2019.00897. Erratum in: Front Neurosci. 2020 Mar 10;14:177. doi: 10.3389/fnins.2020.00177. PMID: 31507369; PMCID: PMC6718611.

Sammons RP, Masserini S, Moreno Velasquez L, Metodieva VD, Cano G, Sannio A, Orlando M, Maier N, Kempter R, Schmitz D. Sub-type specific connectivity between CA3 pyramidal neurons may underlie their sequential activation during sharp waves. Elife. 2025 Aug 15;13:RP98653. doi: 10.7554/eLife.98653. PMID: 40814825; PMCID: PMC12356639.

Sammons RP, Vezir M, Moreno-Velasquez L, Cano G, Orlando M, Sievers M, Grasso E, Metodieva VD, Kempter R, Schmidt H, Schmitz D. Structure and function of the hippocampal CA3 module, Proc. Natl. Acad. Sci. U.S.A. 121 (6) e2312281120, https://doi.org/10.1073/pnas.2312281120 (2024).

Save E, Sargolini F. Disentangling the Role of the MEC and LEC in the Processing of Spatial and Non-Spatial Information: Contribution of Lesion Studies. Front Syst Neurosci. 2017 Oct 27;11:81. doi: 10.3389/fnsys.2017.00081. PMID: 29163076; PMCID: PMC5663729.

Schmidt HG, Rotgans JI, Yew EH. The process of problem-based learning: what works and why. Med Educ. 2011 Aug;45(8):792-806. doi: 10.1111/j.1365-2923.2011.04035.x. PMID: 21752076.

Schmidt-Hieber C, Jonas P, Bischofberger J. Subthreshold dendritic signal processing and coincidence detection in dentate gyrus granule cells. J Neurosci. 2007 Aug 1;27(31):8430-41. doi: 10.1523/JNEUROSCI.1787-07.2007. PMID: 17670990; PMCID: PMC6673070.

Suthana NA, Parikshak NN, Ekstrom AD, Ison MJ, Knowlton BJ, Bookheimer SY, Fried I. Specific responses of human hippocampal neurons are associated with better memory, Proc. Natl. Acad. Sci. U.S.A. 112 (33) 10503-10508, https://doi.org/10.1073/pnas.1423036112 (2015).

Tamamaki N, Nojyo Y. Projection of the entorhinal layer II neurons in the rat as revealed by intracellular pressure-injection of neurobiotin. Hippocampus. 1993 Oct;3(4):471-80. doi: 10.1002/hipo.450030408. PMID: 8269038.

Tervo DG, Hwang BY, Viswanathan S, Gaj T, Lavzin M, Ritola KD, Lindo S, Michael S, Kuleshova E, Ojala D, Huang CC, Gerfen CR, Schiller J, Dudman JT, Hantman AW, Looger LL, Schaffer DV, Karpova AY. A Designer AAV Variant Permits Efficient Retrograde Access to Projection Neurons. Neuron. 2016 Oct 19;92(2):372-382. doi: 10.1016/j.neuron.2016.09.021. Epub 2016 Oct 6. PMID: 27720486; PMCID: PMC5872824.

Thind KK, Yamawaki R, Phanwar I, Zhang G, Wen X, Buckmaster PS. Initial loss but later excess of GABAergic synapses with dentate granule cells in a rat model of temporal lobe epilepsy. J Comp Neurol. 2010 Mar 1;518(5):647-67. doi: 10.1002/cne.22235. PMID: 20034063; PMCID: PMC3098130.

Van Groen T, Miettinen P, Kadish I. The entorhinal cortex of the mouse: organization of the projection to the hippocampal formation. Hippocampus. 2003;13(1):133-49. doi: 10.1002/hipo.10037. PMID: 12625464.

Winnubst J, Bas E, Ferreira TA, Wu Z, Economo MN, Edson P, Arthur BJ, Bruns C, Rokicki K, Schauder D, Olbris DJ, Murphy SD, Ackerman DG, Arshadi C, Baldwin P, Blake R, Elsayed A, Hasan M, Ramirez D, Dos Santos B, Weldon M, Zafar A, Dudman JT, Gerfen CR, Hantman AW, Korff W, Sternson SM, Spruston N, Svoboda K, Chandrashekar J. Reconstruction of 1,000 Projection Neurons Reveals New Cell Types and Organization of Long-Range Connectivity in the Mouse Brain. Cell. 2019 Sep 19;179(1):268-281.e13. doi: 10.1016/j.cell.2019.07.042. Epub 2019 Sep 5. PMID: 31495573; PMCID: PMC6754285.

Witter MP. Intrinsic and extrinsic wiring of CA3: indications for connectional heterogeneity. Learn Mem. 2007 Nov 14;14(11):705-13. doi: 10.1101/lm.725207. PMID: 18007015.

Witter MP. Organization of the entorhinal-hippocampal system: a review of current anatomical data. Hippocampus. 1993;3 Spec No:33-44. PMID: 8287110.

Witter MP, Doan TP, Jacobsen B, Nilssen ES, Ohara S. Architecture of the Entorhinal Cortex A Review of Entorhinal Anatomy in Rodents with Some Comparative Notes. Front Syst Neurosci. 2017 Jun 28;11:46. doi: 10.3389/fnsys.2017.00046. PMID: 28701931; PMCID: PMC5488372.

Witter MP, Groenewegen HJ, Lopes da Silva FH, Lohman AH. Functional organization of the extrinsic and intrinsic circuitry of the parahippocampal region. Prog Neurobiol. 1989;33(3):161-253. doi: 10.1016/0301-0082(89)90009-9. PMID: 2682783.

Wojaczynski GJ, Engel EA, Steren KE, Enquist LW, Patrick Card J. The neuroinvasive profiles of H129 (herpes simplex virus type 1) recombinants with putative anterograde-only transneuronal spread properties. Brain Struct Funct. 2015;220(3):1395-420. doi: 10.1007/s00429-014-0733-9. Epub 2014 Mar 2. PMID: 24585022; PMCID: PMC4152387.

Yassa MA, Stark CE. Pattern separation in the hippocampus. Trends Neurosci. 2011 Oct;34(10):515-25. doi: 10.1016/j.tins.2011.06.006. Epub 2011 Jul 23. PMID: 21788086; PMCID: PMC3183227.

Zhao Y, Jian Y, Liu Z, Liu H, Liu Q, Chen C, Li Z, Wang L, Huang HH, Zeng C. Network Analysis Reveals the Recognition Mechanism for Dimer Formation of Bulb-type Lectins. Sci Rep. 2017 Jun 6;7(1):2876. doi: 10.1038/s41598-017-03003-5. PMID: 28588265; PMCID: PMC5460271.

Zingg B, Dong HW, Tao HW, Zhang LI. Application of AAV1 for Anterograde Transsynaptic Circuit Mapping and Input-Dependent Neuronal Cataloging. Curr Protoc. 2022 Jan;2(1):e339. doi: 10.1002/cpz1.339. PMID: 35044725; PMCID: PMC8852298.

Zingg B, Peng B, Huang J, Tao HW, Zhang LI. Synaptic Specificity and Application of Anterograde Transsynaptic AAV for Probing Neural Circuitry. J Neurosci. 2020 Apr 15;40(16):3250-3267. doi: 10.1523/JNEUROSCI.2158-19.2020. Epub 2020 Mar 20. PMID: 32198185; PMCID: PMC7159884.